PFC/JA-87-20 DOE/ET-51013

A $\vec{k}$-Space Integral Equation for Describing Propagation Through a Strongly Inhomogeneous Plasma Density Profile

R.C. Myer†

MIT Plasma Fusion Center, Cambridge, MA 02139

B.D. Fried‡

Department of Physics, UCLA, Los Angeles, CA 90024

October 16, 1989

† Supported by U.S.D.O.E. Contract DE-AC02-78ET51013.

‡ Supported by U.S.D.O.E. Contract DE-FG03-86ER53225.

ABSTRACT

An integral equation in **k**-space is derived which describes the propagation of electromagnetic waves induced by an external source of charge or current in a magnetized plasma ($\mathbf{B} = B_0\hat{z}$) having an arbitrary density variation in the $\hat{x}$ direction. The nonlocal **k**-space dielectric tensor kernel is derived keeping finite ion Larmor radius (ρ_i) corrections to all orders without the use of an expansion in the inverse density gradient scale length (L_N) so that the effect of a strongly inhomogeneous plasma density profile ($L_N \approx \rho_i$) on ICRF wave propagation can be studied. The integral equation is solved numerically in the electrostatic limit to study the capacitive excitation of ion Bernstein waves for frequencies near the second harmonic of the ion cyclotron frequency ($\omega \approx 2\,\Omega_i$). The spectrum of weakly damped eigenmodes for a plasma having a large region of uniform density and a highly nonuniform edge is found to consist of numerous "uniform plasma" modes and an electrostatic drift mode which propagates only in the edge region. Asymmetries in the radial structure of these modes, which arise from the diamagnetic drift of particles in the plasma edge, result in an asymmetric distribution of wave energy launched in the directions parallel and anti-parallel to the diamagnetic current. The surface electrostatic drift mode is found to be the dominant mode of oscillation as the wave frequency approaches the second harmonic of the ion cyclotron frequency.

I. INTRODUCTION

Plasma heating by radio frequency (RF) electromagnetic waves in the ion cyclotron range of frequencies (ICRF) has a number of applications in plasma confinement experiments. In addition to providing an efficient means of bulk plasma heating,[1] ICRF waves have also been used with some success for impurity control[2] in tokamaks, as well as end loss reduction,[3] and ponderomotive stabilization[4] in mirrors. The effectiveness of ICRF heating in any of these applications relies on an ability to control the RF field profile in the plasma through an appropriate design of the external wave launcher. Since the oscillating electromagnetic field is not directly measurable in fusion plasmas, theoretical models of ICRF heating experiments have been developed to gain an understanding of the influence that antenna geometry, plasma nonuniformities, and kinetic phenomena have on the RF field profile.

For the most part, theoretical models of ICRF wave coupling and propagation have been developed using differential forms of the field equations, in which the plasma response to the RF field is characterized by an equivalent dielectric tensor derived from linear Vlasov theory. A significant simplification which is commonly used to integrate the Vlasov equation is to truncate the Taylor expansion of the perturbed electric field and the equilibrium distribution function about the particle guiding center. The simplest form for the dielectric tensor, that corresponding to a uniform cold plasma, is formally obtained from the Vlasov solution by neglecting terms of order $k_\perp \rho_i$ and ρ_i / L_E, where $k_\perp$ is the perpendicular wavenumber of the perturbed field, ρ_i is the average ion Larmor radius, and L_E is the shortest scalelength associated with the variation of equilibrium parameters. A number of antenna coupling models based on the cold plasma dielectric function have been employed to study the effect of antenna geometry on the global wave field structure in one dimension, using the complete fourth order system of equations,[6-9] and in two dimensions, using a second order system of equations which neglect electron inertia[10,11] ($m_e = 0$). In order to study the effects due to finite temperature or plasma nonuniformities, higher order corrections in $k_\perp \rho_i$ and ρ_i / L_N need to be included; however, the concomitant mathematical complications have limited much of the analysis to one dimensional models which only include first order corrections.

The corrections due to finite Larmor radius (FLR) effects are particularly troublesome since each successive power of $\lambda = (k_\perp \rho_i)^2$ retained in the dielectric function beyond the cold plasma limit raises the order of the wave equation by two. The complexity of the sixth order differential operators which result from including just the first order FLR terms has motivated the development of simpler dielectric models in which specific branches of the dispersion relation are eliminated. For example, in the $m_e = 0$ approximation, the ordinary branch of the dispersion relation is eliminated by assuming that the electric field component

parallel to the magnetic field is zero. While this approximation may be adequate for analyzing certain specific applications, such as fast magnetosonic wave propagation in regions far from the plasma edge, it is not applicable in general, because the ordinary branch corresponds to waves in the plasma periphery which play an important role in the antenna coupling process. Indeed, the $m_e = 0$ approximation has been shown to provide a poor description of slow wave heating experiments in axisymmetric configurations.[8] A number of authors have proposed different schemes for including FLR effects in which the full sixth order equation is solved and the amplitude of the kinetic mode is determined from supplementary boundary conditions, derived by integrating the field equations across the plasma-vacuum interface.[7,12–15] The issue of whether a unique boundary condition scheme exists aside, it may be argued that these models are inappropriate simply because, in reality, there is no well defined plasma-vacuum interface across which boundary conditions can be applied. Moreover, both of these perturbative techniques encounter difficulty when $k_\perp \rho_i \gtrsim 1$ because the transport of such short wavelength field fluctuations by the thermal motion of the plasma particles is an inherently nonlocal process and, as such, is not adequately described by differential equations of finite order.

If the Vlasov equation is integrated without resorting to an expansion in the ion Larmor radius, then the Maxwell-Vlasov equations lead to a system of integro-differential equations. Integral equations have been used to study the eigenmode structure of plasmas with nonuniform density via formulations in both coordinate space[16–18] (x-space) and wavenumber space[19–22] (k-space). The integral equations in x-space treated rather simple, piecewise continuous density profiles while the k-space integral equations have been limited to either Gaussian or parabolic profiles. In this paper, we present a generalization of the k-space integral technique which is fully electromagnetic and is valid for a wide variety of plasma density profiles in slab geometry. In contrast to the previous work on k-space integral equations, we use an integral representation of the Vlasov equilibrium which facilitates the transformation of the equations to k-space.

To simplify the analysis, we assume that the confining magnetic field is uniform. Consequently, this model alone would not be adequate for calculating the global wave structure in complicated equilibria where transverse or parallel magnetic field gradients play an essential role in the wave heating process. Nevertheless, the model should be useful for providing insight into the kinetic phenomena which can occur in the plasma edge, where the effect of the magnetic field gradients can be neglected compared to the gradients in density and temperature. Several recent theoretical models have focused on the role that the edge plasma plays in determining the antenna coupling.[11,15,23] Conditions in the plasma edge, however, preclude an analysis based on the local approximation because the density and temperature

gradient scale lengths in the edge region may be on the order of only a few ion gyroradii, particularly in the scrape-off region behind the plasma limiters. The particle drifts associated with these gradients not only modify the dispersion of the uniform plasma modes, but also give rise to an additional set of electrostatic drift modes which may be excited by the antenna. The direct excitation of these short wavelength ($k_\perp \rho_i \gtrsim 1$) modes may have a detrimental effect on the plasma by altering the power deposition profile or by increasing the radial transport. The advantages of the k-space integral equation formalism over the local differential equation approach in the analysis of this problem are that it includes FLR corrections to all orders and it obviates the need for an expansion of the equilibrium distribution function in powers of ρ_i/L_N. Furthermore, since the integral equation describes the fields in the infinite domain, $x = (-\infty, \infty)$, the illusory issue of plasma-vacuum boundary conditions is entirely circumvented.

The purpose of this paper is to use the $\mathbf{k}-$space integral equation to determine how wave excitation in a plasma slab is affected by the drift currents in the plasma edge. In Section II we describe the model geometry and basic equations. Section III introduces the integral representation of the Vlasov equilibrium solutions and some model profiles which can be considered. Section IV contains the derivation of the linear electromagnetic dielectric tensor kernel for the integral form of the wave equation. In Section V we present some numerical results obtained for the case of ion Bernstein wave excitation by external charge distributions.

II. MODEL GEOMETRY AND BASIC EQUATIONS

Our model assumes a plasma slab that is infinite and uniform in the y and z directions, but has an arbitrary density variation in the x-direction, $n_0 = n_0(x)$. The confining magnetic field is taken to be uniform and in the z direction, $\mathbf{B_0} = B_0\hat{z}$. We consider equilibria which are charge neutral ($\mathbf{E}_0 = 0$) and have $\beta = 8\pi n_0 T/B_0^2 << 1$ so that the magnetic field generated by equilibrium plasma currents may be neglected in comparison to the externally imposed magnetic field. The wave fields, excited by an external source of current and/or charge localized around $x = x_0$ in the low density or "vacuum" region, will be treated as small amplitude perturbations about the equilibrium state.

The plasma is assumed to be collisionless so that its response to the external electromagnetic field is governed by the Vlasov equation

$$\frac{\partial f_\alpha}{\partial t} + \mathbf{v}\cdot\nabla f_\alpha + \frac{q_\alpha}{m_\alpha}(\mathbf{E} + \frac{\mathbf{v}\times\mathbf{B}}{c})\cdot\nabla_v f_\alpha = 0, \tag{1}$$

which describes the evolution of the particle distribution function f_α, for particle species α, with charge q_α, and mass m_α. The electromagnetic field is determined self-consistently from Maxwell's equations

$$\nabla\times\mathbf{E} = -\frac{1}{c}\frac{\partial\mathbf{B}}{\partial t}, \tag{2}$$

$$\nabla\times\mathbf{B} = \frac{4\pi}{c}\mathbf{J} + \frac{1}{c}\frac{\partial\mathbf{E}}{\partial t}, \tag{3}$$

where the current includes an external source, as well as the currents induced in the plasma

$$\mathbf{J} = \mathbf{J}_{ext} + \sum_\alpha q_\alpha \int f_\alpha \mathbf{v} d^3\mathbf{v}. \tag{4}$$

Charge accumulation on the antenna can be permitted by choosing a non-solenoidal current distribution, namely

$$\nabla\cdot\mathbf{J}_{ext} = -\frac{\partial\rho_{ext}}{\partial t} \neq 0.$$

In general, the species subscript, α, will be suppressed except when referring to particular ion or electron quantities, in which case the subscripts "i" or "e" will be used.

III. EQUILIBRIUM SOLUTIONS

Under the assumptions of our model, the Vlasov equation which describes the equilibrium distribution, F_0, of each species is simply

$$v_\perp \cos\phi \frac{\partial F_0}{\partial x} - \Omega \frac{\partial F_0}{\partial \phi} = 0, \tag{5}$$

where $\Omega = qB_0/mc$ is the cyclotron frequency and $v_\perp$ and ϕ are the polar velocity space variables defined by the transformation $v_\perp = (v_x^2 + v_y^2)^{\frac{1}{2}}$ and $\phi = \tan^{-1}(v_y/v_x)$. The general solution to Eq. (5) is any arbitrary function of the variables $v_\perp$, v_z , and the canonical momentum p_y. We consider here distribution functions F_0 which are products of functions of $v_\perp$, v_z, and p_y. For a uniform magnetic field the canonical momentum is just the x-coordinate of the particle guiding center, $p_y = x + v_y/\Omega$. The p_y dependence of F_0 can be chosen to give a specific density variation such as Gaussian, linear, or parabolic. However, to keep the analysis general we use an integral representation[24] of the p_y dependence of F_0

$$F_0 = N_0 F_\perp(v_\perp^2) F_z(v_z) \int_C K(s) e^{is(x+v_y/\Omega)} ds, \tag{6}$$

where $K(s)$ is the integral transform of the guiding center density. Here $F_\perp(v_\perp^2)$ and $F_z(v_z)$ are normalized to unity and the normalization of $K(s)$ is chosen such that N_0 represents the maximum plasma density (i.e, $\int F_0 d^3\mathbf{v} = N_0 g(x)$, where $0 \leq g(x) \leq 1$). One could interpret the integral transform in Eq. (6) as simply a Fourier transform with the contour C taken along the real axis; however, some interesting plasma profiles can be considered by allowing $K(s)$ to be singular and suitably choosing the contour C.

The density profile corresponding to a general distribution of guiding centers is obtained by integrating Eq. (6) over the polar variables $(v_\perp, \phi, v_z)$. The result is

$$n_0(x) = N_0 \int_C e^{isx} K(s) H(s) ds, \tag{7}$$

where

$$H(s) = \int_0^\infty J_0(\frac{sv_\perp}{\Omega}) F_\perp(v_\perp^2) v_\perp dv_\perp, \tag{8}$$

and J_0 is the zero order Bessel function of the first kind. For the purposes of this paper we shall only consider Maxwellian $F_\perp(v_\perp^2) = (\pi v_{th}^2)^{-1} \exp(-v_\perp^2/v_{th}^2)$. In this case, $H(s) = \exp(-s^2\rho^2/4)$ where $\rho = v_{th}/\Omega$ is the average Larmor radius. In the limit of a cold plasma ($\rho = 0$), $H(s) = 1$ and the plasma density coincides with the guiding center density, as it should. When the plasma temperature is not zero, the product $K(s)\exp(-s^2\rho^2/4)$ will generally be narrower than $K(s)$ and, therefore, correspond to a spatial profile in real space which is broader than the guiding center profile due to the thermal motion of the particles.

There are two approaches regarding the choice of $K(s)$. We can specify the density profile $n_0(x)$ and then solve the integral equation given by Eq. (7) to determine the guiding center profile. Alternatively, we can choose an appropriate $K(s)$ and determine the corresponding density by simply evaluating Eq. (7). We have adopted the latter approach for convenience. The simplest choice, $K(s) = \delta(s)$ corresponds to a uniform density profile, $g(x) = 1$. Choosing for $K(s)$ a Gaussian of width $2/w$ and taking the contour C along the real axis we find from Eq. (7) that the corresponding density profile is also a Gaussian, $g(x) = \exp[-x^2/(w^2 + \rho^2)]$. An example of a singular guiding center transform is $K(s) = (2\pi i s)^{-1}$ with the contour C chosen to run below the singularity at $s = 0$. The result is a step-function distribution of guiding centers

$$\begin{aligned} F_0 &= N_0 F_\perp(v_\perp^2) F_z(v_z), \quad && x + v_y/\Omega > 0, \\ F_0 &= 0, && x + v_y/\Omega < 0. \end{aligned} \tag{9}$$

As a result of their gyrating motion, particles can stream into the region $x < 0$ to produce a density profile of the form, $g(x) = \frac{1}{2}[1 + \mathrm{erf}(x/\rho)]$. A simple generalization of this profile is $K(s) = (2\pi i s)^{-1}\exp(-s^2 L_N^2/4)$ which also leads to an error function profile, $g(x) = \frac{1}{2}\{1 + \mathrm{erf}[x/(L_N^2 + \rho^2)^{\frac{1}{2}}]\}$, but with an edge density gradient length which can be varied independently of the plasma temperature. The difference of two error function profiles displaced by $\pm w$, $g(x) = \frac{1}{2}C_n\{\mathrm{erf}[(x + w)/(L_N^2 + \rho^2)^{\frac{1}{2}}] - \mathrm{erf}[(x - w)/(L_N^2 + \rho^2)^{\frac{1}{2}}]\}$, which is obtained by choosing the nonsingular distribution, $K(s) = C_n(\pi s)^{-1}\sin(sw)e^{-s^2 L_N^2/4}$, can be used to model a slab of guiding centers of width $2w$. Here the normalization constant $C_n = [\mathrm{erf}(w/L_N)]^{-1}$ makes $g(0) = 1$. This profile, which we refer to as the double error function (DEF) profile, is an interesting case since it provides a large central region of uniform density where a comparison to local theory can be made and a highly nonuniform edge region where we may expect nonlocal effects to occur. For a given ρ, the DEF profile has two independent scale lengths; w determines the width of the slab and L_N sets the edge scale length.

Although there is considerable freedom in choosing $K(s)$ for a single species, the full set of functions $K_\alpha(s)$ must be chosen to satisfy the charge neutrality condition of the equilibrium. From Eq. (7) it is clear that the plasma density profile will be different for ions and electrons because of the disparity in their Larmor radii. We can guarantee charge neutrality of the equilibrium if we associate with each ion species profile, $K_i(s)$, an electron guiding center profile, $K_e(s)$, satisfying

$$N_{0e} K_e(s) H_e(s) = Z_i N_{0i} K_i(s) H_i(s).$$

IV. THE LINERARIZED WAVE EQUATION IN INTEGRAL FORM

We begin by considering perturbations about the equilibrium described in Section III

$$f = F_0 + f_1(\mathbf{r}, \mathbf{v}, t),$$
$$\mathbf{E} = \mathbf{E}_1(\mathbf{r}, t),$$
$$\mathbf{B} = \mathbf{B}_0 + \mathbf{B}_1(\mathbf{r}, t).$$

Linearizing Eq. (1) and combining Eqs. (2) and (3) we obtain

$$\frac{\partial f_1}{\partial t} + \mathbf{v} \cdot \nabla f_1 + \frac{q}{m} \frac{\mathbf{v} \times \mathbf{B}_0}{c} \cdot \nabla_v f_1 = -\frac{q}{m}\left(\mathbf{E}_1 + \frac{\mathbf{v} \times \mathbf{B}_1}{c}\right) \cdot \nabla_v F_0, \tag{10}$$

$$\nabla \times \left(\nabla \times \mathbf{E}_1\right) + \frac{1}{c^2}\frac{\partial^2 \mathbf{E}_1}{\partial t^2} = -\frac{4\pi}{c^2}\frac{\partial}{\partial t}\left(\mathbf{J}_{ext} + \sum_\alpha q_\alpha \int f_{1\alpha} \mathbf{v} d^3\mathbf{v}\right), \tag{11}$$

where the Laplace-Fourier transform $\widehat{\mathbf{Q}}(\mathbf{k}, \omega)$ of a perturbed quantity, $\mathbf{Q}(\mathbf{r}, t)$, is defined as

$$\widehat{\mathbf{Q}}(\mathbf{k}, \omega) = \int_0^\infty dt \int d^3\mathbf{r}\, \mathbf{Q}(\mathbf{r}, t) e^{-i(\mathbf{k}\cdot\mathbf{r} - \omega t)}, \tag{12}$$

$$\mathbf{Q}(\mathbf{r}, t) = \int_{C_1} \frac{d\omega}{2\pi} \int \frac{d^3\mathbf{k}}{(2\pi)^3}\, \widehat{\mathbf{Q}}(\mathbf{k}, \omega) e^{i(\mathbf{k}\cdot\mathbf{r} - \omega t)}, \tag{13}$$

and the contour C_1 lies below all singularities of $\widehat{\mathbf{Q}}(\mathbf{k}, \omega)$ in the complex ω-plane. Since we shall only be concerned with the time-asymptotic solutions which are steadily oscillating in time, we neglect the initial value terms and set the frequency equal to the frequency of the external drive current, $\widehat{\mathbf{J}}_{ext}(\mathbf{k}, \omega)$. From Eq. (11) we immediately obtain the equation for the transformed electric field

$$\mathbf{k} \times \left(\mathbf{k} \times \widehat{\mathbf{E}}_1(\mathbf{k}, \omega)\right) + \frac{\omega^2}{c^2} \overleftrightarrow{\epsilon} \cdot \widehat{\mathbf{E}}_1(\mathbf{k}, \omega) = -\frac{4\pi i \omega}{c^2} \widehat{\mathbf{J}}_{ext}(\mathbf{k}, \omega), \tag{14}$$

where $\overleftrightarrow{\epsilon}$ is an operator defined by

$$\overleftrightarrow{\epsilon} \cdot \widehat{\mathbf{E}}_1(\mathbf{k}, \omega) = \widehat{\mathbf{E}}_1(\mathbf{k}, \omega) + \frac{4\pi i}{\omega} \sum_\alpha q_\alpha \int \widehat{f}_{1\alpha}(\mathbf{k}, \mathbf{v}, \omega) \mathbf{v} d^3\mathbf{v}. \tag{15}$$

For a uniform plasma equilibrium, the Fourier transformation of Eqs. (10) and (11) yields a k-space dielectric function which is local. That is, the components of the perturbed electric field at any point in k-space can be determined from the system of linear equations in Eq. (14), independent of the values of the perturbed electric field at other points in k-space, since $\widehat{f}_{1\alpha}(\mathbf{k}, \mathbf{v}, \omega)$ is a function of $\widehat{\mathbf{E}}_1(\mathbf{k}, \omega)$ only. Such is not the case for a plasma with nonuniform density, since the spatial dependence of the equilibrium leads to a coupling of the plane wave amplitudes through the dielectric tensor. The derivation of the nonlocal

dielectric function in this case is most easily carried out by using the integral representation of the equilibrium solutions, Eq. (6), when solving Eq. (10) and leaving the s-integration to be performed after the velocity space and trajectory integrations. Equations (14) and (15) then lead to a system of coupled Fredholm integral equations for the components of the Fourier transformed electric field.

Notice that by taking the Fourier transform of Eq. (11) and neglecting the boundary terms to arrive at Eq. (14) we have tacitly imposed the condition that the fields vanish as $|\mathbf{r}| \to \pm\infty$. This is the appropriate boundary condition for a plasma slab of finite extent (i.e., $N_0(x) \to 0$ as $|x| \to \infty$) and for sufficiently low antenna frequency, where the vacuum field is evanescent. Situations where one might expect the time asymptotic solutions to be finite as $|\mathbf{r}| \to \infty$ would be for the idealized case of a semi-infinite plasma with no dissipation or for frequencies high enough that the radiating portion of the antenna power spectrum (i.e., $|\mathbf{k}|^2 < (\omega/c)^2$) is a significant fraction of the total power. Under these circumstances, it is necessary to keep the edge terms and impose outward going radiation conditions.

The perturbed distribution function is obtained by integrating the right hand side of Eq. (10) along the unperturbed particle trajectories

$$f_1(\mathbf{r},\mathbf{v},t) = -\frac{q}{m}\int_{-\infty}^{t} dt' \Big(\mathbf{E}_1 + \frac{\mathbf{v}'\times\mathbf{B}_1}{c}\Big)\cdot\nabla_v F_0, \tag{16}$$

where the particle trajectories, subject to the initial condition, $\mathbf{r}'(t'=t) = \mathbf{r}(t) = (x,y,z)$, are

$$\begin{aligned} x' &= x - \rho\sin[\Omega(t-t')+\phi] + \rho\sin\phi, \\ y' &= y + \rho\cos[\Omega(t-t')+\phi] - \rho\cos\phi, \\ z' &= z - v_z(t-t'). \end{aligned} \tag{17}$$

Transforming Eq. (16) in space and time, using Faraday's law, $\widehat{\mathbf{B}}_1 = (c/\omega)(\mathbf{k}\times\widehat{\mathbf{E}}_1)$, and changing the time integration variable to $\tau = (t-t')$ yields

$$\begin{aligned} \widehat{f}_1(\mathbf{k},\mathbf{v},\omega) = &-\frac{q}{m}N_0 F_\perp F_z \int_0^\infty d\tau e^{i(\omega - k_z v_z)\tau} \\ &\times \int_C ds K(s) e^{i\rho[k_\perp\sin(\phi-\theta) - \widetilde{k}_\perp\sin(\Omega\tau+\phi-\widetilde{\theta})]}\zeta(\tau)\cdot\widehat{\mathbf{E}}_1(\widetilde{\mathbf{k}},\mathbf{v},\omega), \end{aligned} \tag{18}$$

with

$$\zeta_x(\tau) = v_x(\tau)\vartheta_\perp, \tag{19}$$

$$\zeta_y(\tau) = v_y(\tau)\vartheta_\perp + i\frac{s}{\Omega}\Big(1 - \frac{\widetilde{\mathbf{k}}\cdot\mathbf{v}(\tau)}{\omega}\Big), \tag{20}$$

$$\zeta_z(\tau) = \Big[\frac{F_z'}{F_z} - \frac{\widetilde{k}_\perp v_\perp}{\omega}\cos(\Omega\tau+\phi-\widetilde{\theta})\Big(\frac{F_z'}{F_z} - 2v_z\frac{F_\perp'}{F_\perp}\Big) + \frac{isk_y v_z}{\Omega\omega}\Big], \tag{21}$$

$$\vartheta_\perp = \Big[2\frac{F'_\perp}{F_\perp} + \frac{k_z}{\omega}\Big(\frac{F'_z}{F_z} - 2v_z\frac{F'_\perp}{F_\perp}\Big) + \frac{isk_y}{\Omega\omega}\Big], \tag{22}$$

$$\tilde{\mathbf{k}} = (k_x - s, k_y, k_z),$$

$$\tilde{\theta} = \tan^{-1}[k_y/(k_x - s)],$$

$$\theta = \tan^{-1}(k_y/k_x).$$

The two terms in the parentheses of Eqs. (21) and (22) are the usual result of the velocity space gradient in Eq. (16) acting on the perpendicular and parallel velocity distributions. The prime notation here denotes differentiation of these distributions with respect to their arguments, $v_\perp^2$ and v_z, respectively.

The effect of the nonuniform plasma density manifests itself in two ways. First, the terms in Eqs. (19) - (22) that are proportional to "s" are the contributions to the velocity space gradient that arise from the equilibrium diamagnetic drift. For an isotropic Maxwellian distribution, $\vartheta_\perp = -(m/T)(\omega - k_y v_d)/\omega = -(m/T)\omega_D/\omega$ where the quantity ω_D represents the Doppler shifted frequency of the wave in a frame moving in the y-direction with the diamagnetic drift velocity given by, $v_d = isT/m\Omega$. Secondly, the presence of the $\exp(isx)$ factor in the equilibrium distribution shifts the x-component of the Fourier transform variable so that the transformed electric field that appears in Eq. (18) is evaluated at the new wave vector $\tilde{\mathbf{k}}$ which in the x-y plane has the magnitude $\tilde{k}_\perp = [(k_x - s)^2 + k_y^2]^{\frac{1}{2}}$, and is directed radially at the angle $\tilde{\theta}$. The exponential phase factor in Eq. (18) has been written in its most compact form by expressing it in terms of $\tilde{k}_\perp$ and $\tilde{\theta}$.

The plasma current is obtained by performing the velocity integrals of $\hat{f}_1(\mathbf{k}, \mathbf{v}, \omega)$ multiplied by the components of the velocity, $\mathbf{v} = (v_\perp \cos\phi, v_\perp \sin\phi, v_z)$. To facilitate this process we expand the exponential factors in Eq. (18) using the generating function for the Bessel function of the first kind

$$e^{iz\cos\theta} = \sum_{n=-\infty}^{\infty} i^n J_n(z) e^{-in\theta}. \tag{23}$$

The trigonometric τ dependence of $v_x(\tau)$ and $v_y(\tau)$ acts as a raising and lowering operator on the index of the Bessel series corresponding to the $\exp[-i\tilde{k}_\perp\rho\sin(\Omega\tau + \phi - \tilde{\theta})]$ phase factor so that we may rewrite Eq. (18) (after performing the τ-integration) as

$$\hat{f}_1(\mathbf{k}, \mathbf{v}, \omega) = -i\frac{q}{m}N_0 F_\perp F_z \int_C ds K(s) \sum_{l=-\infty}^{\infty} J_l(k_\perp\rho) \sum_{n=-\infty}^{\infty} \frac{\zeta(n)\cdot\hat{\mathbf{E}}_1(\tilde{\mathbf{k}}, \omega) e^{i[l(\phi-\theta)+n(\phi-\tilde{\theta})]}}{(\omega + n\Omega - k_z v_z)}, \tag{24}$$

$$\zeta_x(n) = v_\perp\vartheta_\perp\Big(-iJ'_n(\tilde{k}_\perp\rho)\sin\tilde{\theta} - \frac{nJ_n(\tilde{k}_\perp\rho)}{\tilde{k}_\perp\rho}\cos\tilde{\theta}\Big),$$

$$\zeta_y(n) = v_\perp\vartheta_\perp\Big(\ iJ'_n(\tilde{k}_\perp\rho)\cos\tilde{\theta} - \frac{nJ_n(\tilde{k}_\perp\rho)}{\tilde{k}_\perp\rho}\sin\tilde{\theta}\Big) + \Big(1 + \frac{n\Omega}{\omega} - \frac{k_z v_z}{\omega}\Big)\frac{isT}{\Omega m}J_n(\tilde{k}_\perp\rho),$$

$$\zeta_z(n) = \left[\frac{F_z'}{F_z} + \frac{n\Omega}{\omega}\left(\frac{F_z'}{F_z} - 2v_z\frac{F_\perp'}{F_\perp}\right) + \frac{isk_y v_z}{\Omega\omega}\right] = \vartheta_z J_n(\tilde{k}_\perp\rho).$$

The velocity moments of Eq. (24) can now be performed easily. Multiplying Eq. (24) by the three components of velocity and integrating over ϕ, v_z, and $v_\perp$, substituting the result in Eqs. (14) and (15), and changing the s-integration variable to $\tilde{k}_x = k_x - s$ we arrive at the integral equation for the transformed electric field

$$\mathbf{k}\times\Big(\mathbf{k}\times\widehat{\mathbf{E}}_1(\mathbf{k},\omega)\Big) + \frac{\omega^2}{c^2}\int_C d\tilde{k}_x \overleftrightarrow{\epsilon}(\mathbf{k},\tilde{\mathbf{k}})\cdot\widehat{\mathbf{E}}_1(\tilde{\mathbf{k}},\omega) = -\frac{4\pi i\omega}{c^2}\widehat{\mathbf{J}}_{ext}(\mathbf{k},\omega), \qquad (25)$$

where the dielectric kernel function, $\overleftrightarrow{\epsilon}(\mathbf{k},\tilde{\mathbf{k}})$, for any general distributions, $F_\perp(v_\perp^2)$ and $F_z(v_z)$, is given by Eq. (A2) in the appendix. The components of the dielectric tensor $\overleftrightarrow{\epsilon}$ for an anisotropic Maxwellian ($T_\perp \neq T_z$) which has a nonzero drift velocity in the z-direction (V_s) are given by Eqs. (A3) -(A19) in the appendix.

It is instructive to compare the functional form our dielectric tensor with $K(s) = \delta(s)$ to that of the dielectric tensor for a hot uniform plasma (with $k_y \neq 0$) derived by Swanson.[7] Because of the close similarities between our general dielectric function and the dielectric tensor for the uniform plasma, we have adopted notation similar to Swanson's. For any general $K(s)$, we have defined six functions (K_3, $K_{\perp 1}$, $K_{\perp 2}$, Υ_1, Υ_2, and Υ_3) in addition to those used in the definition of the uniform plasma dielectric. In the limit of a uniform plasma, these functions degenerate as follows, $K_3 \to K_2$, $K_{\perp 1} \to K_{z1}$, and $K_{\perp 2} \to K_{z2}$ so that the functions defined in Eqs. (A4)–(A12) are in exact agreement with those defined in Eqs. (2) - (5) of Swanson's paper with the exception that the displacement current term in our case is removed from the definitions of K_1 and K_{zz} and appears as the delta function $\delta(\tilde{k}_x - k_x)$ in the diagonal elements of $\overleftrightarrow{\epsilon}$. The equivalence of $K_{\perp 1}$ and $K_{\perp 2}$ to K_{z1} and K_{z2} is evident from the relations

$$\sum_{n=-\infty}^{\infty}\langle\Theta_z\rangle_n n\Lambda_{n\alpha} = \sum_{n=-\infty}^{\infty}\langle\Theta_\perp t\rangle_n n\Lambda_{n\alpha},$$

$$\sum_{n=-\infty}^{\infty}\langle\Theta_z\rangle_n(\Lambda_{n\alpha} - \Lambda'_{n\alpha}) = \sum_{n=-\infty}^{\infty}\langle\Theta_\perp t\rangle_n(\Lambda_{n\alpha} - \Lambda'_{n\alpha}),$$

which hold only when $\tilde{\theta} = \theta$. These relations follow from Eq. (A18) and the property $I_{-n}(\lambda_\alpha) = I_n(\lambda_\alpha)$ for integer values of n. The functions Υ_1, Υ_2, and Υ_3 vanish in the uniform plasma limit and have no corresponding term in the uniform plasma dielectric as they represent modifications of the plasma response due to the equilibrium drifts. Evidently, these terms represent a fluid drift response since the Z-function is absent in their definition.

The dielectric tensor for a hot uniform plasma possesses the symmetry property

$$\epsilon_{ij}(\mathbf{k};-B_0) = \epsilon_{ji}(\mathbf{k};B_0),$$

which is the generalized Onsager relation derived from arguments regarding the thermodynamics of irreversible processes.[25-27] It is therefore surprising at first sight that the components of the dielectric tensor for a hot nonuniform plasma do not possess this symmetry, as is clearly evident by the presence of the drift terms Υ_1, Υ_2, and Υ_3 and the fact that $K_{\perp 1} \neq K_{z1}$ and $K_{\perp 2} \neq K_{z2}$. However, the derivation of the Onsager relations from the theory of fluctuations is based on the assumption that the set of fluctuations which characterize the deviation of the system from thermostatic equilibrium are independent variables.[27] This assumption is invalid for a hot nonuniform plasma since the set of variables which describe the deviation from equilibrium (in our case, the values of $\widehat{\mathbf{E}}_1(\tilde{\mathbf{k}},\omega)$ along the contour C) are linearly related (Eq. (25)) thus, the nonlocal dielectric function should not be expected to possess the Onsager symmetry.

An integral equation for the Fourier transformed electrostatic potential, $\widehat{\phi}_1(\mathbf{k},\omega)$, is obtained by forming the scalar product of $\mathbf{k}$ with Eq. (25) and replacing $\widehat{E}_1(\tilde{\mathbf{k}},\omega)$ by $-i\tilde{\mathbf{k}}\widehat{\phi}_1(\tilde{\mathbf{k}},\omega)$. This operation contracts the dielectric tensor to a simple scalar function and the driving term, $\widehat{J}_{ext}(\mathbf{k},\omega)$, is replaced by the charge distribution on the antenna, $\widehat{\rho}_{ext}(\mathbf{k},\omega)$. The result is

$$(k_x^2+k_y^2+k_z^2)\widehat{\phi}_1(\mathbf{k},\omega)+\sum_\alpha \frac{\omega_{p\alpha}^2 m_\alpha}{T_{\perp\alpha}}\int_C d\tilde{k}_x \widehat{\phi}_1(\tilde{\mathbf{k}},\omega)K_\alpha(k_x-\tilde{k}_x)\sum_{n=-\infty}^{\infty}\Lambda_{n\alpha} \qquad (26)$$
$$\times\left[1+(\xi_{D\alpha}-\frac{\mathrm{V}_{s\alpha}}{\mathrm{V}_{z\alpha}})Z(\chi_{n\alpha})+\frac{1}{2}Z'(\chi_{n\alpha})(1-\frac{T_{\perp\alpha}}{T_{z\alpha}})\right]=4\pi\widehat{\rho}_{ext}(\mathbf{k},\omega),$$

where for each species α we define the quantities $\Lambda_{n\alpha}(\lambda_\alpha) = I_n(\lambda_\alpha)e^{-\beta_\alpha}e^{in(\tilde{\theta}-\theta)}$, $\lambda_\alpha = k_\perp\tilde{k}_\perp T_{\perp\alpha}/(m_\alpha\Omega_\alpha^2), \beta_\alpha = (k_\perp^2+\tilde{k}_\perp^2)T_{\perp\alpha}/(2m_\alpha\Omega_\alpha^2)$, and $\chi_{n\alpha} = \xi_{n\alpha} - \mathrm{V}_{s\alpha}/\mathrm{V}_{z\alpha}$. There are two limits for which the integral equation can be easily solved analytically. First, in the limit, $T_{\perp\alpha} = T_{z\alpha} \to 0$, the kernel in Eq. (26) reduces to a function of $(k_x - \tilde{k}_x)$ only so that the integral equation can be solved, using the convolution theorem, to yield the differential equation

$$\left[-\frac{d^2}{dx^2}+k_y^2+k_z^2-\sum_\alpha\omega_{p\alpha}^2\left(\frac{k_z^2}{\omega^2}g_\alpha(x)+\frac{k_y g_\alpha'(x)}{\Omega_\alpha\omega}\right)\right]\widehat{\phi}_1(x,k_y,k_z,\omega)=4\pi\widehat{\rho}_{ext}(x,k_y,k_z,\omega),$$

where $g_\alpha(x)$ is the normalized plasma density profile for species α. Secondly, when $K(s) = \delta(s)$, Eq. (26) reduces to $|\mathbf{k}|^2\epsilon_L\widehat{\phi}_1(\mathbf{k},\omega) = 4\pi\widehat{\rho}_{ext}(\mathbf{k},\omega)$ where ϵ_L is the usual electrostatic dielectric function for an infinite plasma.[28] In general, the kernel in Eq. (26) is a function of both k_x and $\tilde{k}_x$, reducing to neither a product of functions of k_x and $\tilde{k}_x$ (degenerate kernel) nor a function of $k_x - \tilde{k}_x$ alone. For a Gaussian profile, $K(s) = \mathrm{e}^{-(sw)^2/4}$, the left hand side of Eq. (26) is identical to the result derived by Watanabe et al.,[20] but does not agree with the electrostatic integral equation derived by Sivasubramanian and Tang.[19]

These authors treated the spatial dependence of the equilibrium incorrectly, introducing the nonuniform density after the trajectory integrals were performed rather than constructing a proper equilibrium distribution from the constants of motion.

Since Eq. (26) is an integral equation in k_x, the quantities k_y, k_z, and ω play the role of free parameters. Omitting the explicit dependence of these parameters, we write Eq. (26) in the form

$$a(k_x)\widehat{\phi}_1(k_x) + \int_{-\infty}^{\infty} \mathrm{M}(k_x, \tilde{k}_x)\widehat{\phi}_1(\tilde{k}_x)d\tilde{k}_x = f(k_x). \tag{27}$$

We cannot solve this equation analytically for situations that are of interest so we approximate the integral by a discrete sum over a suitable finite interval $[a, b]$ on the real k_x axis to obtain the matrix equation

$$\sum_{j=1}^{N} A_{ij}\,\widehat{\phi}_1(k_j) \equiv \sum_{j=1}^{N}\Big(a(k_j)\delta_{i,j} + \mathrm{M}(k_i, k_j)w_j\Big)\,\widehat{\phi}_1(k_j) = f(k_i), \tag{28}$$

which we can solve numerically. Here the points k_j $(j = 1, N)$ are the abscissae and w_j the associated weight factors for a particular N-point quadrature formula (e.g., trapezoidal, Simpson, or Gauss). In the limit $N \to \infty$, the approximate solution $\widehat{\phi}_1(k_j)$ will tend to the exact solution of Eq. (27) provided that Eq. (28) has a unique solution.[29] The well known condition for this is just that A_{ij} is nonsingular, that is, $\Delta = \det A_{ij} \neq 0$. Restoring the dependence of the solution on the free parameters, we obtain from Cramer's rule

$$\widehat{\phi}_1(x, k_y, k_z, \omega) = (2\pi)^{-1} \sum_{j=1}^{N} \frac{\Delta_j(k_y, k_z, \omega)}{\Delta(k_y, k_z, \omega)} e^{ik_j x} w_j, \tag{29}$$

where $\Delta_j(k_y, k_z, \omega)$ is the determinant of the matrix obtained by replacing the j-th column of A_{ij} with the vector $f(k_i)$.

To find $\widehat{\phi}_1(x, y, z, \omega)$ we need to perform the remaining integrals over k_y and k_z. As k_y and k_z are varied it is possible to encounter points in the (k_y, k_z, ω) parameter space where $\Delta(k_y, k_z, \omega) = 0$. This is just the condition that the homogenous equation associated with Eq. (28) have a non-trivial solution, which implies that the inhomogeneous solution, Eq. (29), is not unique. These poles of $\widehat{\phi}_1(x, k_y, k_z, \omega)$ correspond to the normal modes of the plasma slab. Although Eq. (29) gives the correct spatial structure for the normal modes, that being the coefficient of $(2\pi\Delta)^{-1}$, it does not give the normal mode amplitudes correctly since the inhomogeneous solution increases without bound as we approach the poles of $\widehat{\phi}_1(x, k_y, k_z, \omega)$. To determine the amplitude of each mode excited by the antenna, which we expect to be finite due to the presence of damping, we perform the integration along a contour which is deformed about the poles of $\widehat{\phi}_1(x, k_y, k_z, \omega)$. Leaving k_z fixed for the moment, we note that if the antenna has finite extension in y, then the integration of Eq. (29) over k_y, after

multiplication by the phase factor $\exp(ik_y y)/2\pi$, can, for large $|y|$, be expressed in terms of the residues of $[\Delta(k_y, k_z, \omega)]^{-1}$

$$\widehat{\phi}_1(x, y, k_z, \omega) = \sum_l \sum_{j=1}^{N} \widehat{\phi}_r(k_j, k_l, k_z, \omega) e^{i(k_j x + k_l y)} w_j, \tag{30}$$

where

$$\widehat{\phi}_r(k_j, k_l, k_z, \omega) = i \frac{\Delta_j(k_l, k_z, \omega)}{\Delta'(k_l, k_z, \omega)},$$

and $\Delta'(k_y, k_z, \omega)$ is the derivative of the determinant with respect to k_y. Here the sum of the residues extends over those roots of the determinant ($\Delta(k_l, k_z, \omega) = 0$) for which $\mathrm{Re}(k_l)y > 0$. The z variation of the field can be obtained by integrating Eq. (30) over k_z after multiplication by the phase factor $\exp(ik_z z)/2\pi$. The reader is cautioned that the analytic continuation of the $Z-$function from positive to negative values of $Re(k_z)$ introduces a branch cut in the complex k_z plane which must be properly included in the complete reconstruction of the field. Alternatively, we could reverse the order of the k_y and k_z integrals to obtain the solution for large $|z|$ involving a sum over the residues in the complex k_z-plane and an integral over k_y. Since the diamagnetic drift frequency is proportional to k_y, we expect the effect of the plasma edge to be most evident in the k_y eigenmode spectrum and have, therefore, followed the former approach in obtaining the numerical solutions presented in the next section.

V. NUMERICAL SOLUTIONS: BERNSTEIN WAVE COUPLING

In this section we present numerical solutions to Eq. (26) for frequencies near the second harmonic of the ion cyclotron frequency ($\omega \approx 2\,\Omega_i$). Our primary goal is to study the direct excitation of electrostatic plasma waves, in particular, the ion Bernstein waves, by an external source of charge and to determine the effect of the edge plasma on antenna coupling. The results presented here are for a hydrogen plasma with Maxwellian ions and electrons, $T_{\perp\alpha} = T_{z\alpha}$, $V_{s\alpha} = 0$, $T_i = T_e$, and $\omega_{pe}/\Omega_e = 2$. All plasma and antenna parameters are expressed in dimensionless form. The ion Bernstein waves (IBW) are excited by an oscillating surface charge density on localized conducting surfaces such as the antenna itself or a Faraday shield. Taking the charge density to be confined to an infinitely thin layer on the surface of an infinite planar conductor located at $x = x_0$, we make the replacement $\rho_{ext}(\mathbf{r}) = \delta(x - x_0)\sigma_{ext}(y, z)$. For simplicity, we take the external charge distribution to be a line of charge with a sinusoidal variation in the z-direction, ie., $\sigma_{ext}(y, z) = \delta(y)\exp(i2\pi z/L_z)$ or $\hat{\sigma}_{ext}(\mathbf{k}, \omega)\rho_i^2 = \delta(k_z - 2\pi/L_z)$, which gives equal weighting to the k_y spectrum of waves for fixed k_z. Of course, a detailed comparison of this model to any particular experiment would require that the full k_z integration be carried out for a specific antenna geometry. Our intention here is merely to examine the changes in the k_y spectrum due to variations in ω, k_z, and the plasma density profile.

The computational requirements for solving the integral equation are determined mainly by the number of points (N_k) used in the numerical integration scheme, with the memory requirements scaling as N_k^2 and the execution time (determined primarily by the number of steps needed to invert a fully populated matrix by direct methods) scaling as N_k^3. For a given set of plasma conditions, the optimal integration parameters may be found by increasing the integration interval in k_x until the Fourier transformed potential, $\widehat{\phi}_1(k_x, k_y, k_z, \omega)$, is sufficiently small at the endpoints that the error due to truncation of the integral may be neglected. The number of points in the integration scheme is chosen such that an increase in the number of points (for a fixed integration interval) beyond N_k does not significantly alter the solution. For most of the results presented in this section, we find that a trapezoidal quadrature scheme using 101 abscissae on the interval $k_x\rho_i = [-1, 1]$ is adequate. The matrix equation is solved directly using the method of LU decomposition (IMSL routine LEQ2C) and the spatial profiles are obtained by inverse Fourier transformation using the same trapezoidal quadrature formula. Typical execution time for calculating and inverting the 101-by-101 matrix is about 3 seconds on the Cray-XMP.

We first present the numerical results for the double error function (DEF) profile with a half-width $w = 50\,\rho_i$ and an edge scale length $L_N = 5\,\rho_i$. Since the density gradient is

very weak in the center of the DEF profile, we expect that the wave propagation there will be accurately described by the IBW dispersion relation for a uniform plasma. We examine this first, since it provides both a check on the numerical solution of the integral equation and a useful basis for a qualitative understanding of the numerical results.

Choosing $k_z\rho_i = 2 \times 10^{-3}$ and convenient values of $k_y\rho_i$ from 0 to 0.3, we solve $\Delta = 0$ to find the eigenvalues of ω and the associated eigenvectors, $\widehat{\phi}_1(x, k_y, k_z, \omega)$. For each set of k_y and ω we find the shape of $\widehat{\phi}_1(x, k_y, k_z, \omega)$ from Eq. (29). An approximate value of k_x is determined by measuring the separation between the nodes of $\widehat{\phi}_1(x, k_y, k_z, \omega)$ in the central region of the slab. The discrete k_y eigenmodes are displayed as the points in Fig. 1. The solid curves show the variation of k_x with ω/Ω_i as predicted by the uniform plasma IBW dispersion relation for the plasma parameters at the center of the DEF profile and the indicated values of $k_y\rho_i$.

The points in Fig. 2 are determined by the same process, save that we fix ω, solve $\Delta = 0$ to find the k_y eigenvalues, and plot the k_x values, obtained again from graphs of $\widehat{\phi}_1(x, k_y, k_z, \omega)$ versus x in the central region, against the corresponding k_y. The resultant points in the k_x-k_y plane fall on the circles (solid curves in Fig. 2) predicted from the uniform plasma IBW dispersion relation using the central plasma parameters. The horizontal axis in Fig. 2 is $|k_y|\rho_i$ since the distribution of eigenvalues is symmetric about $k_y = 0$. Figures 1 and 2 clearly demonstrate that the wave structure in the center of the DEF profile indeed obeys the IBW dispersion relation for a uniform plasma, as expected.

Figure 3 displays the spatial structure of some of the eigenmodes for $\omega = 1.95\ \Omega_i$, $k_z\rho_i = 2. \times 10^{-3}$, and the indicated values of the eigenvalue $k_y\rho_i$. The solid curves in these figures represent the real part of the electrostatic potential while the chaindot curves, which are plotted relative to the right hand axes, display the normalized plasma density profile, $g(x)$. The imaginary part of the potential is not plotted here since its amplitude is three orders of magnitude lower than the real part. Notice that the peak amplitude of each eigenmode presented here has been normalized to unity. The two outermost peaks in Figs. 3(a)-3(e), which we will refer to as the cutoff peaks, arise from the Airy-like pattern associated with the reflection of the IBW from the vacuum region where the field is evanescent. The waves are weakly damped for the conditions assumed here since the arguments of the Z-functions in the kernel for both ions and electrons are large, $\xi_{0e} \approx \xi_{-2i} \approx 25 \gg 1$. Hence, both electron Landau damping and ion cyclotron damping are completely negligible and the field structure in the center of the plasma, established by multiple reflections of the IBW between the two cutoff peaks, resembles a cavity mode. The slight ripple in the field which occurs outside of the two cutoff peaks is due to numerical errors introduced by the the truncation of the k_x integration.

The curves in Figs. 3(a)-3(e) show, in the order of increasing $k_y\rho_i$, the spatial structure of the first, fifth, tenth, eleventh, and twelfth eigenmodes lying on curve (e) in Fig. 2. Notice that the drift induced asymmetry of the field is enhanced for the (lower/higher) order (k_x/k_y) modes. On the basis of uniform plasma theory, we expect k_x to decrease with increasing k_y until $k_x w \approx \pi/2$ (approximately one half wavelength fitting in the slab), as is the case in Fig. 3(e). For larger values of k_y the transverse wavelength exceeds the plasma width and the wave should be cutoff. However, an additional mode, shown in Fig. 3(f), was found for values of k_y slightly larger than its expected cutoff value. This mode, which is highly nonlocal in k-space ($k_x L_N \approx 2\pi$), exhibits behavior characteristic of an electrostatic drift mode in that it requires a density gradient to propagate (oscillatory in the x-direction) and it propagates in only one direction relative to the diamagnetic drifts. Since $\omega/k_y > 0$, this mode propagates in a direction parallel to the electron diamagnetic drift of the edge plasma at $x = +w$. The mode for $k_y\rho_i \approx -.393$ has a spatial structure which is the mirror image of that in Fig. 3(f) and corresponds to a wave propagating in the edge plasma at $x = -w$ where the electron diamagnetic drift is reversed.

The most significant feature of the mode structure, from the standpoint of antenna coupling, is the asymmetry of the mode structure in the edge regions. The asymmetry arises from the drift term $\xi_{D\alpha}$ in Eq. (26) which effectively changes the particle response to the field by Doppler shifting the wave frequency upward or downward depending on the sign of k_y and the direction of the density gradient. To a very good approximation, the shape, $\widehat{\phi}_1(x)$, of any weakly damped mode with $k_y < 0$ is simply the mirror image of its $k_y > 0$ counterpart, since the anti-Hermitian part of the integral operator in Eq. (26) arises primarily from the drift term. As a consequence, the asymmetric structure of the cutoff peaks can lead to an asymmetric excitation between the $k_y > 0$ and the $k_y < 0$. waves. To assess the importance of this asymmetric excitation we must determine how the coupled energy is distributed among the various eigenmodes. The total, time-averaged work performed on the plasma is

$$\begin{aligned}\overline{W} &= \int d^3\mathbf{r}\, \mathbf{J}(\mathbf{r},\omega)\cdot\mathbf{E}^*(\mathbf{r},\omega),\\ &= \frac{-i\omega}{32\pi^4}\int dk_x \widehat{\phi}_1^*(k_x)\int d\tilde{k}_x \widehat{\phi}_1(\tilde{k}_x)\Big(\mathbf{k}^*\cdot\overleftrightarrow{\epsilon}(k_x,\tilde{k}_x)\cdot\tilde{\mathbf{k}} - \mathbf{k}^*\cdot\tilde{\mathbf{k}}\delta(k_x-\tilde{k}_x)\Big)\end{aligned}$$

Approximating the integral by a sum and using Eq. (30) we have

$$\begin{aligned}\overline{W} &= \frac{-i\omega}{32\pi^4}\int dk_z \sum_l \sum_{i=1}^{N}\sum_{j=1}^{N} \widehat{\phi}_r^*(k_i,k_l,k_z,\omega)\widehat{\phi}_r(k_j,k_l,k_z,\omega)K(k_i,k_j)w_i w_j,\\ &= \int dk_z \sum_l W(k_l,k_z),\end{aligned}$$

where $W(k_l,k_z)$ is the energy per unit k_z associated with the normal mode $k_y = k_l$. In

subsequent figures we plot, for given k_z and ω, $\log_{10}[W(k_l, k_z)/W_{\max}]$, where $W_{\max}$ is the largest of $W(k_l, k_z)$.

Figure 4 shows the power spectrum for an antenna located at $x = 60\,\rho_i$ with $\omega/\Omega_i = 1.95, 1.97$, and 1.99. The modes shown in Figs. 4(a)-4(c) are the same "uniform plasma" modes lying on the curves labeled (e), (c), and (a), respectively in Fig. 2. The solid points correspond to modes having $k_y > 0$, circles to modes with $k_y < 0$. In each case, the two modes having the largest value of k_y are the drift modes which are confined to the plasma edge region. The overall shape of the power spectrum depends sensitively on the antenna location relative to the cutoff peaks. For example, if the antenna lies outside of the cutoff peak for the IBW, then the coupling amplitude is primarily determined by the distance from the antenna to the cutoff peak and the vacuum field e-folding distance for each mode. On the other hand, if the antenna lies inside the cutoff peak, then the coupling amplitude is determined by the position of the antenna relative to the locations of the nodes and anti-nodes of the eigenmode structure, these locations being independent of the antenna position. For the cases shown in Fig. 4, the $k_y > 0$ modes are preferentially excited because the antenna at $x = 60\,\rho_i$ lies near the maximum of the cutoff peak for the modes, but outside of the cutoff peak for the $k_y < 0$ modes.

The power spectrum in Fig. 4(a) is typical for situations where the wave frequency is far from an ion cyclotron resonance, $\xi_{ni} \gg 1$. Generally, the modes on the low end of the k_y power spectrum are preferentially excited because the vacuum field scale length for these modes is longer (in vacuum $k_x = \pm i(k_y^2 + k_z^2)^{\frac{1}{2}}$). These modes also exhibit a higher degree of symmetry since the diamagnetic drift term, being proportional to k_y, has a diminished influence in determining the mode structure. Thus, from the spectrum in Fig. 4(a) we conclude that the spatial structure of the far field of the antenna to be essentially that shown in Fig. 3(a) with roughly equal amounts of wave energy launched in the $\pm\hat{y}$ directions. The sequence of Figs. 4(a)-4(c) show that as the wave frequency approaches the second harmonic of the ion cyclotron frequency the asymmetry in the power spectrum of the "uniform plasma" modes increases and the amplitude of the surface drift mode relative to the rest of the spectrum steadily increases. Notice that the surface drift mode is the dominant mode in Fig. 4(c) where $\omega/\Omega_i = 1.99$. For these conditions the antenna far field would be similar to Fig. 3(f) with most of the wave energy propagating in the direction of the electron diamagnetic drift in the edge closest to the antenna. The amplitude of the surface drift mode is enhanced by the single particle resonance of ions in the plasma edge. The resonance of ions gyrating in the edge is analogous to the Azbeĺ-Kaner resonance of electrons in metals which occurs when the penetration length of an electromagnetic field applied at the surface is comparable to the electron gyroradius.[30]

The effect of the diamagnetic drift is increased for waves having a shorter parallel wavelength or for plasmas having a steeper gradient. Figure 5 shows that decreasing the parallel wavelength results in eigenmode power spectra which are more asymmetric, particularly for the lower order k_x modes. The structure of the eigenmodes for $k_z\rho_i = 10^{-2}$, Fig. 6(c), is similar to that of the modes in Fig. 3. However, the mode asymmetry is enhanced due to an increase in the amplitude of the cutoff peak at $x = +w$ relative to the rest of the eigenmode structure. We also find that the $k_\perp$ of the excited waves increases with increasing k_z, as indicated by the extension of the k_y spectrum in Fig. 5. The increase in $k_\perp$ is most dramatic for the surface drift mode which shifts to higher values of $|k_y|$ much faster than the rest of the spectrum. An increased mode asymmetry and increased $|k_y|$ is also observed for the surface drift mode as L_N is reduced.

All of the eigenmodes considered thus far have been weakly damped since $\xi_{ni} >> 1$ and $\xi_{0e} >> 1$ with the result that $\mathrm{Im}(k_y) \ll \mathrm{Re}(k_y)$. Under these circumstances, the Fourier reconstruction of the field may be conveniently separated into two distinct parts; the contribution from the contour which represents the near field of the antenna and the contribution from the poles which represents the far field. For cases where $\xi_{ni} \lesssim 1$ (ion cyclotron damping) or $\xi_{0e} \approx 1$ (electron Landau damping) the poles move off the real k_y axis (which corresponds to spatial damping of the waves) and the distinction between the near and far field is no longer meaningful. Here the field may be reconstructed by performing the k_y integration along the real k_y axis. As an example of such a situation, we consider a case with $\xi_{-2i} \lesssim 1$ where ion cyclotron damping effects are important. Figures 6(a) and 6(b) show the reconstructed potential profile for a plasma having the same parameters as that in Fig. 3, but with $\omega/\Omega_i = 1.99$ and $k_z\rho_i = .004$ and .008, respectively. The k_y integration in each case was performed with a 101 point trapezoidal integration scheme along the real axis on the interval $k_y\rho_i = [-1., 1.]$. The spurious oscillations in the vacuum region are attributed to numerical errors due to the crude integration scheme employed here. When integrating over k_y we find that the width of the spectrum in k_x space varies considerably. As a consequence, there are values of k_y for which the k_x grid introduces noticeable errors. These errors could be eliminated by dynamically changing both the width and number of points of the k_x grid. The peaks in the potential profiles shown in Figs. 6(a) and 6(b) are broadened by the varying location of the cutoff peaks as k_y is varied. Spatial damping of the field is evident from the decrease in the amplitude of the wave as it propagates away from the antenna ($x_0/\rho_i = 60$) and the fact that the potential has acquired a complex part comparable to its real part. The k_y power spectrum for the two cases are shown on the same relative scale in Fig. 6(c). The most interesting feature of these spectra is the dramatic asymmetry about $k_y = 0$ of roughly three orders of magnitude. The peaks on curve (a) are due to the presence of the poles lying

near the real axis which correspond to the most weakly damped modes. As k_z increases the poles move further from the real axis resulting in a smoothing of the power spectrum as can seen by comparing curve (b). The relative magnitude of the k_y power spectra decreases monotonically as k_z increases beyond these values.

We find that the surface drift mode retains its drift-like character as the density gradient scale length of the edge plasma is increased (ie., propagating only in the region with a density gradient and only in the direction of the electron diamagnetic drift) even when the density gradient scale length is comparable to the size of the plasma, as in the case of a Gaussian profile. Figures 7(a)-7(c) show the lowest order k_x modes for a plasma with the same peak density as before and $k_z\rho_i = 2. \times 10^{-3}$, but with a Gaussian profile having a scale length $L_N = 30\,\rho_i$. As before, the modes having $k_y < 0$ are the mirror image of the modes displayed in Fig. 7. The lowest order mode, Fig. 7(a), which has only a slight asymmetry about $x = 0$, is the remaining vestige of the surface drift mode. The enhanced asymmetry of the lowest order k_x modes when $k_z\rho_i = 10^{-2}$ can be seen in the results of Figs 7(d)-7(f). The three modes shown are propagating (real k_x) in the region $x > 0$ and evanescent in the region $x < 0$ where the direction of the diamagnetic current is reversed. The evanescence of the field is not due to absorption since the imaginary part of the potential is still several orders of magnitude lower than the real part. The k_y power spectra for modes in a Gaussian profile, for various values of $k_z\rho_i$, are shown in Fig. 8. The drift induced asymmetry of the power spectra is less systematic for the Gaussian profile than for the DEF profile due to larger variations in the location of the cutoffs and nodes relative to the antenna. As we have seen before, increasing k_z increases the extent of the k_y spectra and also enhances the power spectra asymmetry. Notice that the power coupled to the lower k_x modes increases with increasing k_z to the point where the spectrum is nearly flat for the $k_y > 0$ modes when $k_z\rho_i = 10^{-2}$.

Ferraro and Fried[31] have studied diamagnetic drift effects on IBW propagation in a plasma slab with a Gaussian profile for frequencies between the first and second harmonic using a differential equation approach. Because their infinite order differential equation was truncated at second order, reliable solutions were only obtained for frequencies in the range $1 \lesssim \omega/\Omega_i \lesssim 1.7$. Nevertheless, their calculations indicate effects similar to those presented here, including the asymmetries in wave amplitude and wavenumber in the direction along the density gradient. Although the solution in $x-$space provides more physical intuition into how the wave properties change with the plasma parameters, it is difficult to extend this approach to higher frequencies because of the algebraic complexity involved in deriving the coefficients of the differential equation.

VI. CONCLUSION

We have derived the k-space integral equation governing electromagnetic wave propagation in a nonuniform plasma and have used it to investigate some of the nonlocal effects associated with ICRF antenna coupling. The dielectric kernel function was derived as a natural extension of the dielectric function for a uniform plasma through the use of an integral representation of the Vlasov equilibrium. The derivation of the k-space integral equation keeps FLR corrections to all orders without resorting to an expansion based on the weakness of the density gradient and is, therefore, valid for frequencies near the higher harmonics of the ion cyclotron frequency and for a wide variety of plasma density profiles.

The direct excitation of electrostatic waves by capacitive coupling to an external source of charge was examined by numerical solution of the integral equation. Eigenmode profiles were obtained for frequencies in the range of the second harmonic of the ion cyclotron frequency and for various parallel wavelengths. In regions of very weak density variation, the dispersive properties of the excited plasma waves are found to agree closely with those of the ion Bernstein wave in a uniform plasma. In addition to the eigenmodes one would expect on the basis of a uniform plasma model, which are cut off when k_y exceeds a critical value, k_c, an electrostatic drift which propagates in a direction parallel to the electron diamagnetic drift and is localized to the edge region was found to exist for values of $k_y > k_c$. This mode, which is not predicted by local analysis since it has both $k_\perp \rho \approx 1$ and $k_x L_N \approx 2\pi$, maintains its drift-like character even when the density scale length is comparable to the size of the plasma (as in the case of the Gaussian profile). In both of the plasma profiles considered here, the electrostatic drift modes are found to be the dominant mode of oscillation as $\omega \rightarrow 2\Omega_i$.

The diamagnetic drift current which exists in the plasma edge region is found to produce an asymmetric eigenmode structure that can lead to asymmetric distribution of power between the $k_y > 0$ and $k_y < 0$ modes. The mode asymmetry is particularly important for modes having larger values of k_y and k_z and for plasmas having very steep density gradients at the plasma edge. Similar strong asymmetries are observed in the k_y power spectrum when the launched waves are strongly damped. These results may have implications for ICRF experiments since the asymmetric distribution of power between the $k_y > 0$ and $k_y < 0$ modes, which in more realistic geometries would correspond to propagation in the azimuthal or poloidal direction, may result in nonuniform (up-down asymmetry) power deposition profiles. The amount of the asymmetry in the power spectrum will depend sensitively on the location of the antenna relative to the cutoff layers and the details of the plasma edge profile.

APPENDIX: THE LINEAR ELECTROMAGNETIC KERNEL

For a general class of separable Vlasov equilibria of the form,

$$F_0 = N_0 F_\perp(v_\perp^2) F_z(v_z) \int_C K(s) e^{is(x+v_y/\Omega)} ds,$$

the integral equation in k-space for the perturbed electric field is,

$$\mathbf{k} \times \Big(\mathbf{k} \times \widehat{\mathbf{E}}_1(\mathbf{k},\omega) \Big) + \frac{\omega^2}{c^2} \int_C d\tilde{k}_x \overleftrightarrow{\epsilon}(\mathbf{k},\tilde{\mathbf{k}}) \cdot \widehat{\mathbf{E}}_1(\tilde{\mathbf{k}},\omega) = -\frac{4\pi i\omega}{c^2} \widehat{\mathbf{J}}_{ext}. \tag{A1}$$

where,

$$\begin{aligned}
\overleftrightarrow{\epsilon}(\mathbf{k},\tilde{\mathbf{k}}) \cdot \widehat{\mathbf{E}}_1(\tilde{\mathbf{k}},\omega) = \delta(\tilde{k}_x - k_x)\widehat{\mathbf{E}}_1(\mathbf{k},\omega) + \sum_\alpha \Big(\frac{\omega_{p\alpha}}{\Omega_\alpha}\Big)^2 K_\alpha(k_x - \tilde{k}_x) \sum_{n=-\infty}^{\infty} 4 \int_0^\infty r\, dr \\
\Big\{ \widehat{E}_x r \Big(\frac{-nJ_n(\tilde{\gamma}_\alpha r)}{\tilde{\gamma}_\alpha r} \cos\tilde{\theta} - iJ_n'(\tilde{\gamma}_\alpha r) \sin\tilde{\theta} \Big) \frac{\langle \Theta_{\perp\alpha} \mathcal{I} \rangle_n}{\mathrm{V}_{\perp\alpha}} F_{\perp\alpha}(r^2) \\
+ \widehat{E}_y r \Big[\Big(\frac{-nJ_n(\tilde{\gamma}_\alpha r)}{\tilde{\gamma}_\alpha r} \sin\tilde{\theta} + iJ_n'(\tilde{\gamma}_\alpha r) \cos\tilde{\theta} \Big) \frac{\langle \Theta_{\perp\alpha} \mathcal{I} \rangle_n}{\mathrm{V}_{\perp\alpha}} F_{\perp\alpha}(r^2) \\
+ \frac{i}{2}(k_x - \tilde{k}_x) \frac{\mathrm{V}_{\perp\alpha}}{\Omega_\alpha} J_n(\tilde{\gamma}_\alpha r) \pi \mathrm{V}_{\perp\alpha}^2 F_{\perp\alpha}(r^2) \int_{-\infty}^{\infty} \frac{\mathrm{V}_{z\alpha} F_{z\alpha}(t) \mathcal{I}}{\mathrm{V}_{\perp\alpha}} dt \Big] \\
+ \widehat{E}_z J_n(\tilde{\gamma}_\alpha r) \frac{\langle \Theta_{z\alpha} \mathcal{I} \rangle_n}{\mathrm{V}_{z\alpha}} F_{\perp\alpha}(r^2) \Big\}.
\end{aligned} \tag{A2}$$

The dielectric tensor is a function of the two wavevectors $\mathbf{k} = (k_\perp \cos\theta, k_\perp \sin\theta, k_z)$ and $\tilde{\mathbf{k}} = (\tilde{k}_x, k_y, k_z) = (\tilde{k}_\perp \cos\tilde{\theta}, \tilde{k}_\perp \sin\tilde{\theta}, k_z)$. The perpendicular wavenumbers, perpendicular kinetic velocity ($v_\perp$), and parallel kinetic velocity (v_z) in Eq. (A2) are all normalized to the perpendicular ($\mathrm{V}_{\perp\alpha}$) and parallel ($\mathrm{V}_{z\alpha}$) thermal velocities, namely, $\gamma_\alpha = k_\perp \mathrm{V}_{\perp\alpha}/\Omega_\alpha$, $\tilde{\gamma}_\alpha = \tilde{k}_\perp \mathrm{V}_{\perp\alpha}/\Omega_\alpha$, $r = v_\perp/\mathrm{V}_{\perp\alpha}$, and $t = v_z/\mathrm{V}_{z\alpha}$. We have also defined the following functions,

$$\begin{aligned}
\Theta_{\perp\alpha} &= -\frac{1}{2}\xi_{0\alpha}\pi^{\frac{3}{2}} \Big[2\frac{F_\perp'}{F_\perp} + \frac{k_z}{\omega}\Big(\frac{F_z'}{F_z} - 2v_z\frac{F_\perp'}{F_\perp}\Big) + \frac{i(k_x - \tilde{k}_x)k_y}{\Omega\omega} \Big]_\alpha, \\
\Theta_{z\alpha} &= -\frac{1}{2}\xi_{0\alpha}\pi^{\frac{3}{2}} \Big[\frac{F_z'}{F_z} + \frac{n\Omega}{\omega}\Big(\frac{F_z'}{F_z} - 2v_z\frac{F_\perp'}{F_\perp}\Big) + \frac{i(k_x - \tilde{k}_x)k_y v_z}{\Omega\omega} \Big]_\alpha, \\
\mathcal{I}(n) &= (2\pi)^{-1} \int_0^{2\pi} \sum_{l=-\infty}^{\infty} J_l(k_\perp \rho) e^{il(\phi-\theta)} e^{in(\phi-\tilde{\theta})} \mathbf{v}\, d\phi, \\
\langle Q(t) \rangle_n &= \pi^{-\frac{1}{2}} \int_{-\infty}^{\infty} \frac{Q(t) F_z(t)\, dt}{t - \xi_{n\alpha}}, \\
\xi_{n\alpha} &= (\omega + n\Omega)/k_z \mathrm{V}_{z\alpha}.
\end{aligned}$$

If we assume a drifting bi-Maxwellian velocity distribution for species α ($\mathrm{V}_{\perp\alpha}^2 = 2T_{\perp\alpha}/m_\alpha$ and $\mathrm{V}_{z\alpha}^2 = 2T_{z\alpha}/m_\alpha$),

$$F_{\perp\alpha}(v_\perp^2) F_{z\alpha}(v_z) = (\pi^{\frac{3}{2}} \mathrm{V}_{\perp\alpha}^2 \mathrm{V}_{z\alpha})^{-1} e^{-(v_\perp/\mathrm{V}_{\perp\alpha})^2} e^{-[(v_z - \mathrm{V}_{s\alpha})/\mathrm{V}_{z\alpha}]^2}$$

then the components of the dielectric tensor kernel are of the form,

$$
\begin{aligned}
\epsilon_{xx} &= K_1\cos(\tilde{\theta}-\theta) + 2K_0\sin\tilde{\theta}\sin\theta - (K_2\sin\tilde{\theta}\cos\theta - K_3\cos\tilde{\theta}\sin\theta) + \delta(\tilde{k}_x - k_x),\\
\epsilon_{xy} &= K_2\cos\tilde{\theta}\cos\theta + K_3\sin\tilde{\theta}\sin\theta - 2K_0\cos\tilde{\theta}\sin\theta + K_1\sin(\tilde{\theta}-\theta)\\
&\quad + \Upsilon_1\cos\theta - \Upsilon_2\sin\theta,\\
\epsilon_{xz} &= K_{\perp 1}\cos\theta + K_{\perp 2}\sin\theta,\\
\epsilon_{yx} &= -(K_2\sin\tilde{\theta}\sin\theta + K_3\cos\tilde{\theta}\cos\theta + 2K_0\sin\tilde{\theta}\cos\theta) - K_1\sin(\tilde{\theta}-\theta),\\
\epsilon_{yy} &= K_1\cos(\tilde{\theta}-\theta) + 2K_0\cos\tilde{\theta}\cos\theta - (K_2\cos\tilde{\theta}\sin\theta - K_3\sin\tilde{\theta}\cos\theta)\\
&\quad + \Upsilon_1\sin\theta + \Upsilon_2\cos\theta + \delta(\tilde{k}_x - k_x),\\
\epsilon_{yz} &= K_{\perp 1}\sin\theta - K_{\perp 2}\cos\theta,\\
\epsilon_{zx} &= K_{z1}\cos\tilde{\theta} - K_{z2}\sin\tilde{\theta},\\
\epsilon_{zy} &= K_{z1}\sin\tilde{\theta} + K_{z2}\cos\tilde{\theta} + \Upsilon_3,\\
\epsilon_{zz} &= K_{zz} + \delta(\tilde{k}_x - k_x).
\end{aligned}
\tag{A3}
$$

The functions in the dielectric tensor are,

$$K_1 = \sum_\alpha \left(\frac{\omega_{p\alpha}}{\omega}\right)^2 K_\alpha(k_x-\tilde{k}_x)\sum_{n=-\infty}^{\infty}\frac{n^2\Lambda_{n\alpha}}{\lambda_\alpha}\langle\Theta_\perp\rangle_n, \tag{A4}$$

$$K_{zz} = -\sum_\alpha \left(\frac{\omega_{p\alpha}}{\omega}\right)^2 K_\alpha(k_x-\tilde{k}_x)\sum_{n=-\infty}^{\infty}\Lambda_{n\alpha}\langle\Theta_z t\rangle_n, \tag{A5}$$

$$K_2 = \sum_\alpha \left(\frac{\omega_{p\alpha}}{\omega}\right)^2 K_\alpha(k_x-\tilde{k}_x)\sum_{n=-\infty}^{\infty} in\left(\frac{\tilde{k}_\perp}{k_\perp}\Lambda_{n\alpha} - \Lambda'_{n\alpha}\right)\langle\Theta_\perp\rangle_n, \tag{A6}$$

$$K_3 = \sum_\alpha \left(\frac{\omega_{p\alpha}}{\omega}\right)^2 K_\alpha(k_x-\tilde{k}_x)\sum_{n=-\infty}^{\infty} in\left(\frac{k_\perp}{\tilde{k}_\perp}\Lambda_{n\alpha} - \Lambda'_{n\alpha}\right)\langle\Theta_\perp\rangle_n, \tag{A7}$$

$$K_0 = \sum_\alpha \left(\frac{\omega_{p\alpha}}{\omega}\right)^2 K_\alpha(k_x-\tilde{k}_x)\sum_{n=-\infty}^{\infty}\left(\lambda_\alpha\Lambda_{n\alpha} - \beta_\alpha\Lambda'_{n\alpha}\right)\langle\Theta_\perp\rangle_n, \tag{A8}$$

$$K_{z1} = \sum_\alpha \left(\frac{\omega_{p\alpha}}{\omega}\right)^2 K_\alpha(k_x-\tilde{k}_x)\left(\frac{T_{z\alpha}}{T_{\perp\alpha}}\right)^{\frac{1}{2}}\sum_{n=-\infty}^{\infty}\frac{n\Lambda_{n\alpha}}{\tilde{\gamma}_\alpha}\langle\Theta_\perp t\rangle_n, \tag{A9}$$

$$K_{z2} = i\sum_\alpha \left(\frac{\omega_{p\alpha}}{\omega}\right)^2 K_\alpha(k_x-\tilde{k}_x)\left(\frac{T_{z\alpha}}{T_{\perp\alpha}}\right)^{\frac{1}{2}}\sum_{n=-\infty}^{\infty}\left(\gamma_\alpha\Lambda_{n\alpha} - \tilde{\gamma}_\alpha\Lambda'_{n\alpha}\right)\langle\Theta_\perp t\rangle_n, \tag{A10}$$

$$K_{\perp 1} = \sum_\alpha \left(\frac{\omega_{p\alpha}}{\omega}\right)^2 K_\alpha(k_x-\tilde{k}_x)\left(\frac{T_{\perp\alpha}}{T_{z\alpha}}\right)^{\frac{1}{2}}\sum_{n=-\infty}^{\infty}\frac{n\Lambda_{n\alpha}}{\gamma_\alpha}\langle\Theta_z\rangle_n, \tag{A11}$$

$$K_{\perp 2} = i\sum_\alpha \left(\frac{\omega_{p\alpha}}{\omega}\right)^2 K_\alpha(k_x-\tilde{k}_x)\left(\frac{T_{z\alpha}}{T_{\perp\alpha}}\right)^{\frac{1}{2}}\sum_{n=-\infty}^{\infty}\left(\tilde{\gamma}_\alpha\Lambda_{n\alpha} - \gamma_\alpha\Lambda'_{n\alpha}\right)\langle\Theta_z\rangle_n, \tag{A12}$$

$$\Upsilon_1 = \frac{i(k_x-\tilde{k}_x)}{k_\perp}\sum_\alpha \left(\frac{\omega_{p\alpha}}{\omega}\right)^2 K_\alpha(k_x-\tilde{k}_x)\sum_{n=-\infty}^{\infty} n\Lambda_{n\alpha}, \tag{A13}$$

$$\Upsilon_2 = \frac{(k_x - \tilde{k}_x)}{k_\perp} \sum_\alpha \Big(\frac{\omega_{p\alpha}}{\omega}\Big)^2 K_\alpha(k_x - \tilde{k}_x) \sum_{n=-\infty}^{\infty} \lambda_\alpha \Big(\Lambda'_{n\alpha} - \frac{k_\perp}{\tilde{k}_\perp}\Lambda_{n\alpha}\Big) \tag{A14}$$

$$\Upsilon_3 = \frac{i}{2} \sum_\alpha \Big(\frac{\omega_{p\alpha}}{\omega}\Big)^2 K_\alpha(k_x - \tilde{k}_x) \sum_{n=-\infty}^{\infty} \Lambda_{n\alpha} \frac{(k_x - \tilde{k}_x)\mathrm{V}_s}{\Omega_\alpha} \tag{A15}$$

$$\langle \Theta_\perp \rangle_n = (\xi_{D\alpha} - \frac{V_s}{V_z}) Z(\chi_{n\alpha}) + \frac{1}{2} Z'(\chi_{n\alpha})(1 - \frac{T_{\perp\alpha}}{T_{z\alpha}}), \tag{A16}$$

$$\langle \Theta_\perp t \rangle_n = Z'(\chi_{n\alpha}) \Big[\xi_{D\alpha} - (1 - \frac{T_{\perp\alpha}}{T_{z\alpha}})\xi_{n\alpha}\Big] + 2\frac{\mathrm{V}_{s\alpha}}{\mathrm{V}_{z\alpha}} \Big[1 - Z(\chi_{n\alpha})(\xi_{D\alpha} - \xi_{n\alpha})\Big], \tag{A17}$$

$$\langle \Theta_z \rangle_n = \frac{T_{z\alpha}}{T_{\perp\alpha}} \langle \Theta_\perp t \rangle_n + \frac{\mathrm{V}_{s\alpha}}{\mathrm{V}_{z\alpha}}, \tag{A18}$$

$$\langle \Theta_z t \rangle_n = \frac{T_{z\alpha}}{T_{\perp\alpha}} \Big\{ \xi_{n\alpha} Z'(\chi_{n\alpha}) \Big[(1 - \frac{T_{\perp\alpha}}{T_{z\alpha}})\xi_{n\alpha} - \xi_{D\alpha}\Big] + 2\frac{\mathrm{V}_{s\alpha}}{\mathrm{V}_{z\alpha}} (\xi_{D\alpha} - \xi_{n\alpha}) \Big[1 + \xi_{n\alpha} Z(\chi_{n\alpha})\Big] \Big\} \tag{A19}$$

Other quantities which appear in Eqs. (A4) -(A19) are defined as follows,

$$\Lambda_{n\alpha}(\lambda_\alpha) = I_n(\lambda_\alpha) e^{-\beta_\alpha} e^{in(\tilde{\theta} - \theta)}, \qquad \lambda_\alpha = k_\perp \tilde{k}_\perp T_{\perp\alpha}/(m_\alpha \Omega_\alpha^2),$$
$$\beta_\alpha = (k_\perp^2 + \tilde{k}_\perp^2) T_{\perp\alpha}/(2 m_\alpha \Omega_\alpha^2), \quad \chi_{n\alpha} = \xi_{n\alpha} - \mathrm{V}_{s\alpha}/\mathrm{V}_{z\alpha},$$
$$\omega_{D\alpha} = \omega + \frac{i(\tilde{k}_x - k_x) k_y T_{\perp\alpha}}{m_\alpha \Omega_\alpha}, \qquad \Omega_\alpha = q_\alpha B_0/m_\alpha c,$$
$$\xi_{D\alpha} = \omega_{D\alpha}/(k_z \mathrm{V}_{z\alpha}), \qquad \omega_{p\alpha} = (4\pi N_{0\alpha} q_\alpha^2/m_\alpha)^{\frac{1}{2}}.$$

where, $I_n(\lambda_\alpha)$ is the modified Bessel function of the first kind and $Z(\xi)$ is the plasma dispersion function[32],

$$Z(\xi) = \pi^{-\frac{1}{2}} \int_{-\infty}^{\infty} \frac{e^{-t^2} dt}{t - \xi}.$$

The prime notation in Eqs. (A4)–(A19) denotes differentiation with respect to the argument of the function.

ACKNOWLEDGEMENTS

The authors gratefully acknowledge useful discussions with Dr. Robert Ferraro whose work on the infinite order differential equation describing electrostatic waves in nonuniform plasma slabs contributed greatly to the interpretation of the results presented here. This work was supported in part by U.S. DOE Contract DE-AC02-78ET51013.

FIGURE CAPTIONS

Figure 1. Frequency dispersion of the slab plasma eigenmodes for $k_y\rho_i =$ (a) 0., (b) .1, (c) .2, and (d) .3 .

Figure 2. k_y dispersion of the slab plasma eigenmodes for $\omega/\Omega_i =$ (a) 1.99, (b) 1.98, (c) 1.97, (d) 1.96, and (e) 1.95 .

Figure 3. The real part of the electrostatic potential (solid curve) and the normalized density, $g(x)$, (chaindot curve) versus x/ρ_i. Approximate values of $k_y\rho_i$ are: (a) .0823, (b) .291, (c) .372, (d) .378, (e) .382, and (f) .393 .

Figure 4. The eigenmode power spectra for the DEF profile with $k_z\rho_i = .002$ for $\omega/\Omega_i = (a)1.95$, (b) 1.97, and (c) 1.99. The solid points coorespond to modes having $k_y > 0$ while the circles correspond to modes having $k_y < 0$.

Figure 5. The eigenmode power spectra for the DEF profile with $\omega/\Omega_i = 1.95$ and $k_z\rho_i =$(a) .002, (b) .005, and (c) .01.

Figure 6. The electrostatic potential profile and normalized density versus x/ρ_i for $\omega/\Omega_i = 1.99$ and $k_z\rho_i =$ (a) .004 and (b) .008. The solid and dashed curves represent the real and imaginary parts of the potential, respectively. Figure (c) shows the relative k_y spectra for figures (a) and (b).

Figure 7. The real part of the electrostatic potential and the normalized density versus x/ρ_i. Approximate values of the wavenumbers are $k_z\rho_i = 2. \times 10^{-3}$ with $k_y\rho_i =$ (a).383, (b).377, (c).370, and $k_z\rho_i = 10^{-2}$ with $k_y\rho_i =$ (d).421, (e).415, and (f).408.

Figure 8. The eigenmode power spectra for the Gaussian profile with $\omega/\Omega_i = 1.95$ and $k_z\rho_i =$ (a) .002, (b) .005, and (c) .01.

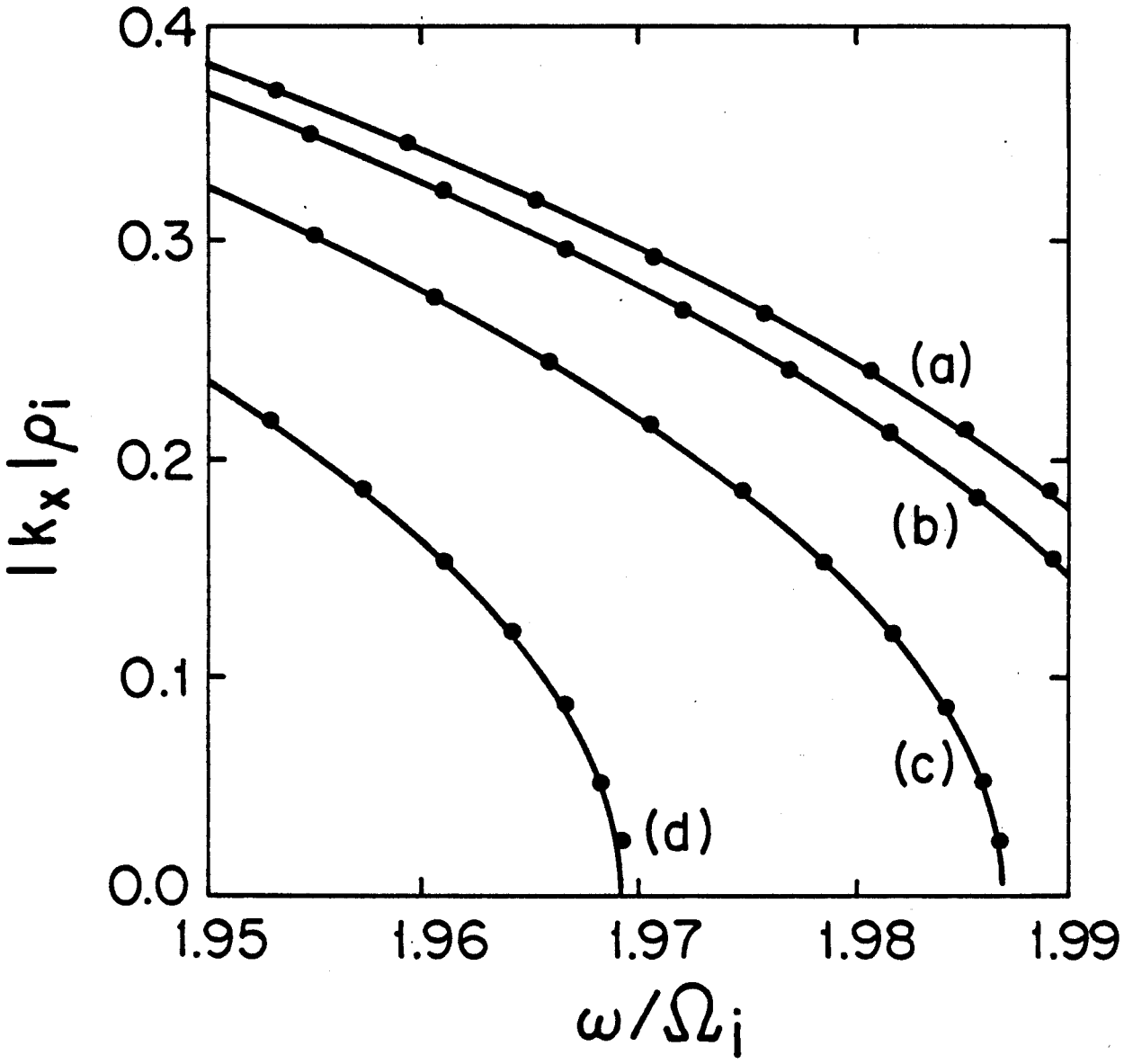

Figure 1

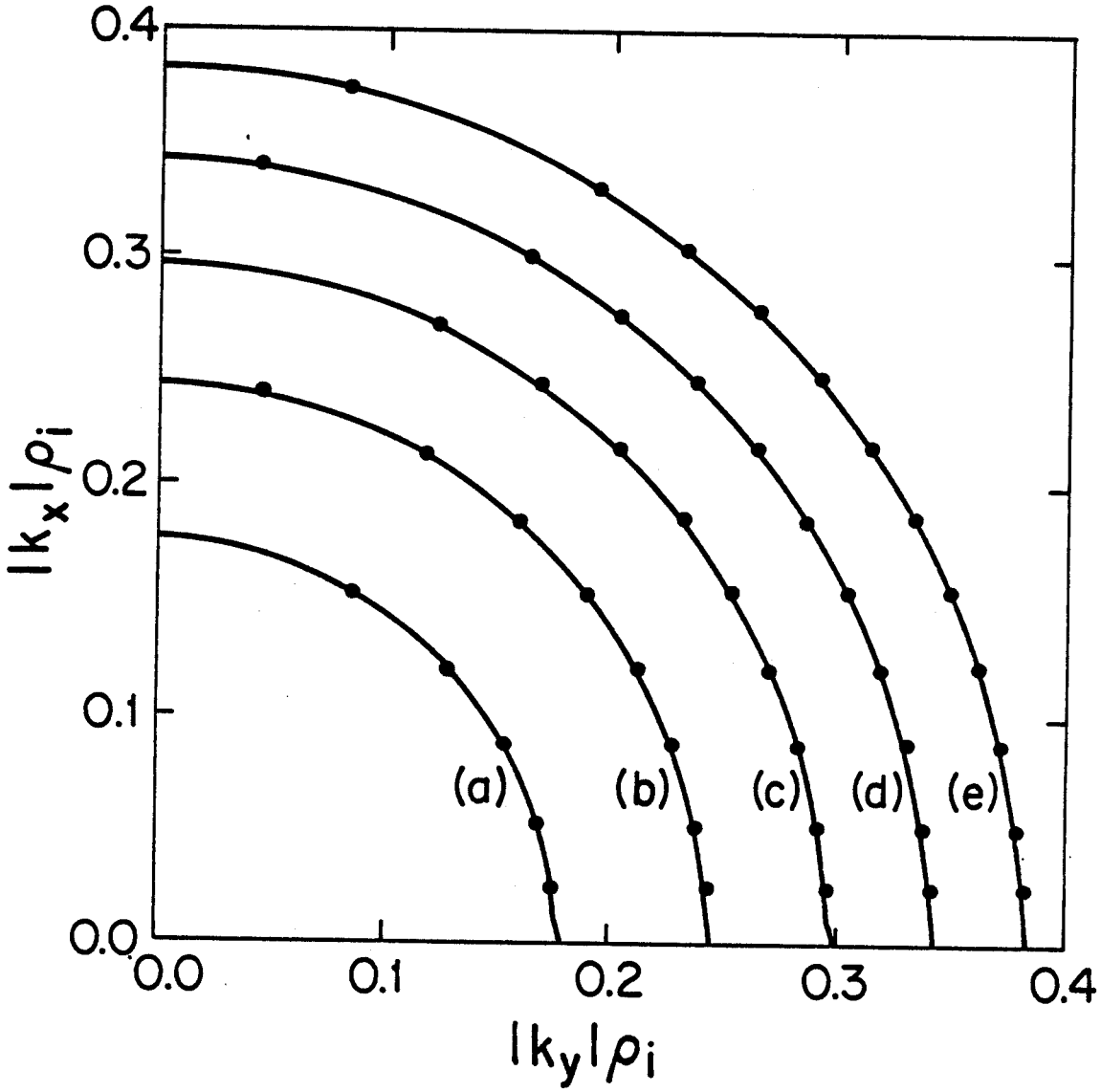

Figure 2

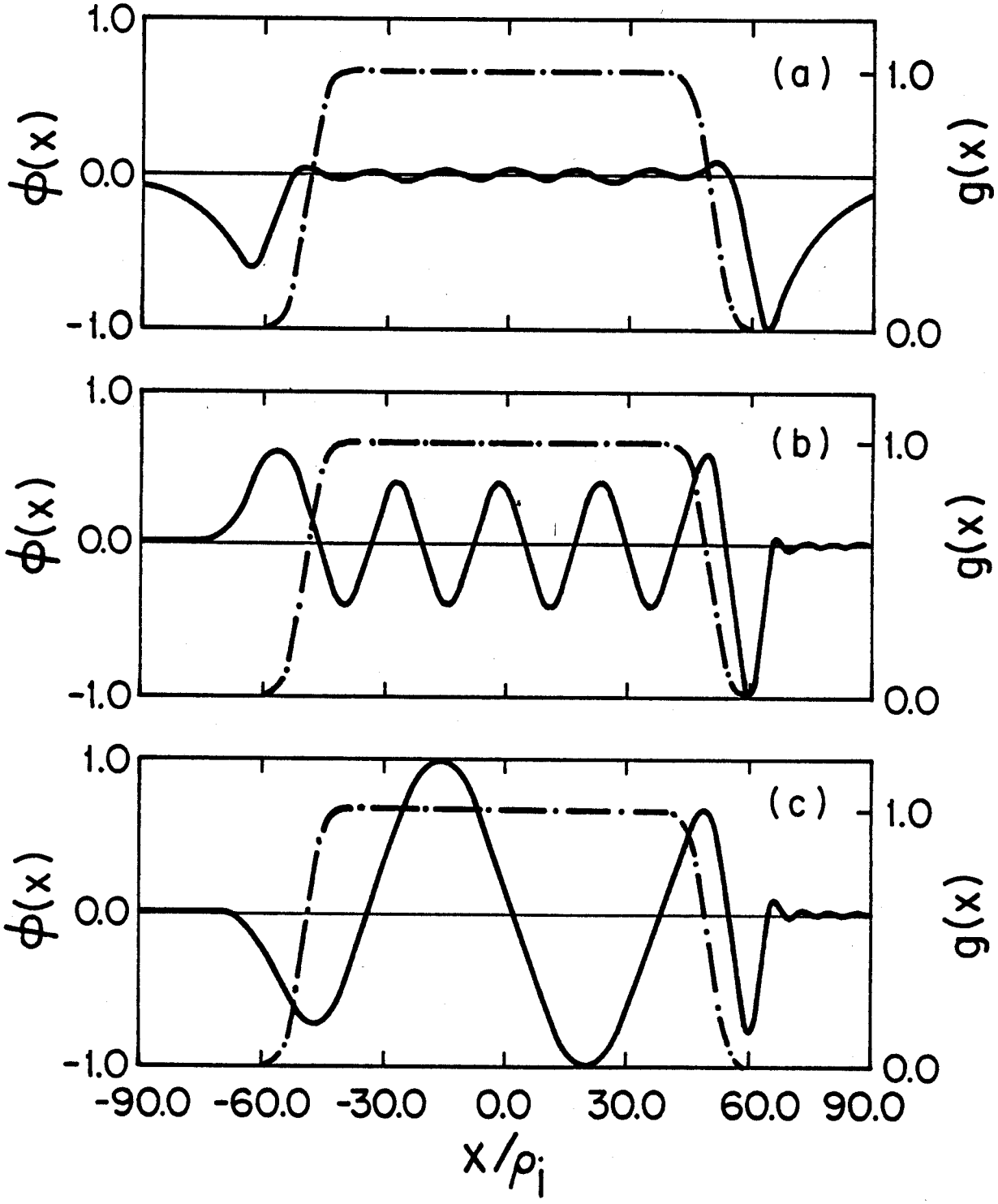

Figure 3

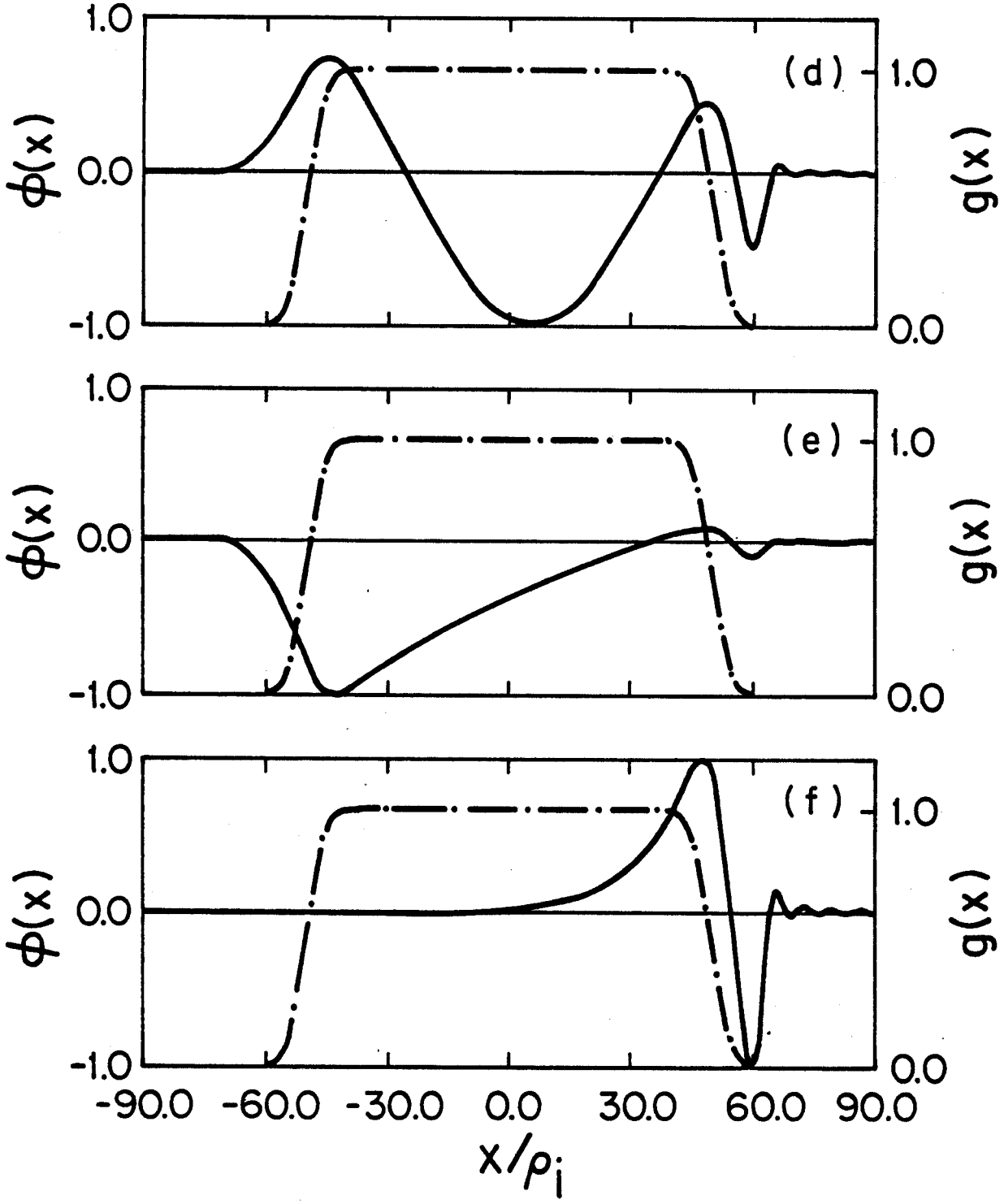

Figure 3

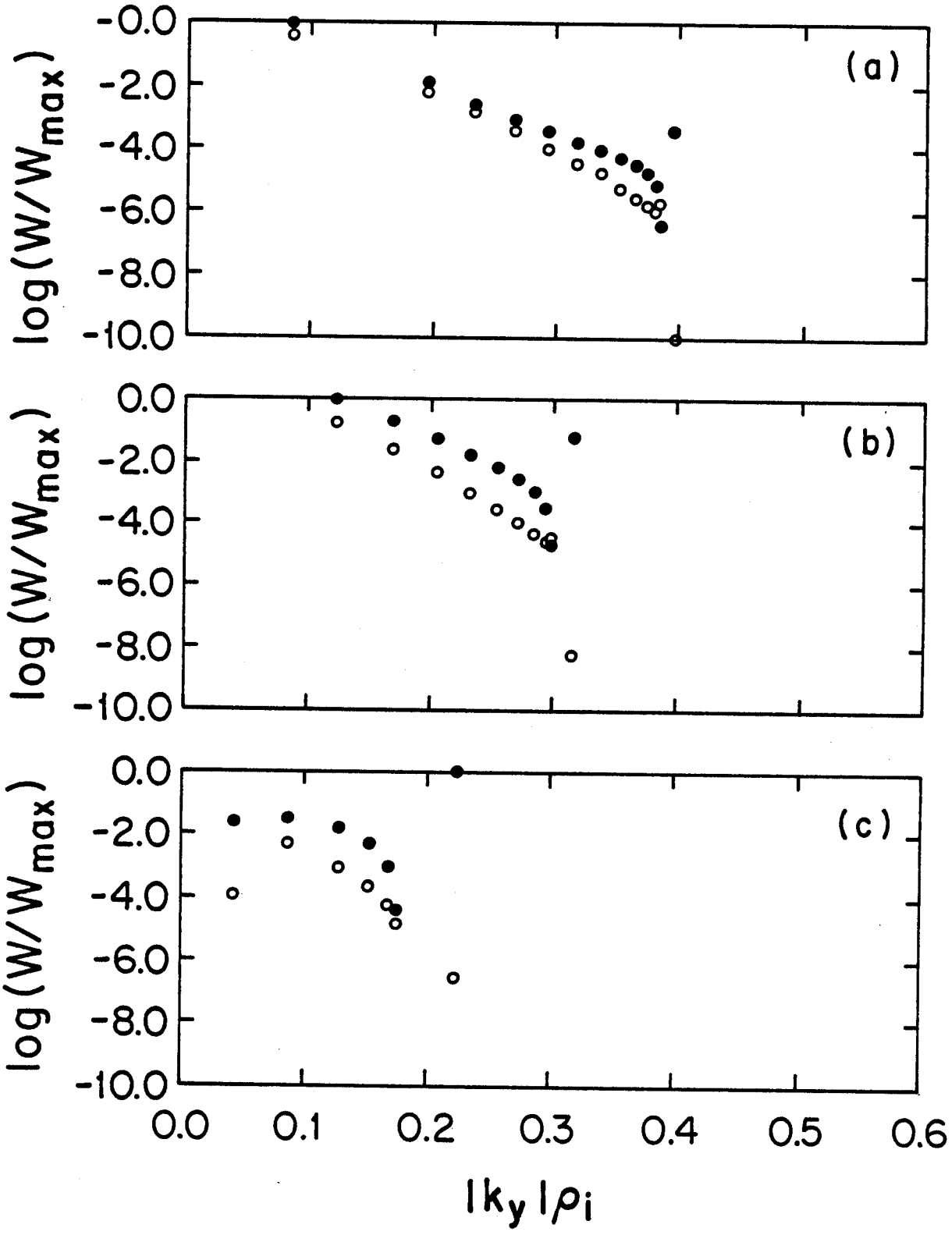
-0.0
-2.0
-4.0
-6.0
-8.0
-10.0
log(W/W_max)
(a)
0.0
-2.0
-4.0
-6.0
-8.0
-10.0
log(W/W_max)
(b)
0.0
-2.0
-4.0
-6.0
-8.0
-10.0
log(W/W_max)
(c)
0.0
0.1
0.2
0.3
0.4
0.5
0.6
|k_y|ρ_i

Figure 4

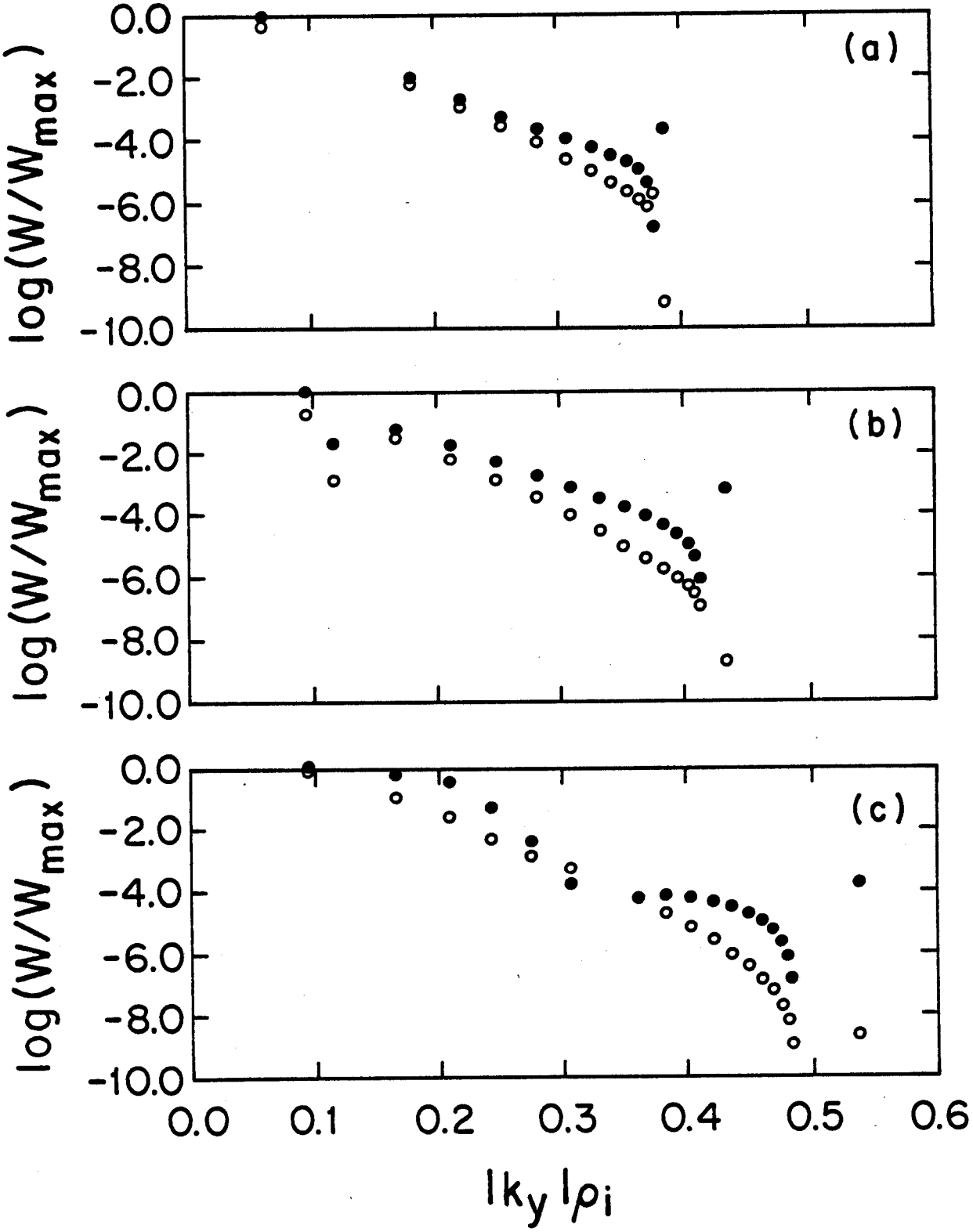

Figure 5

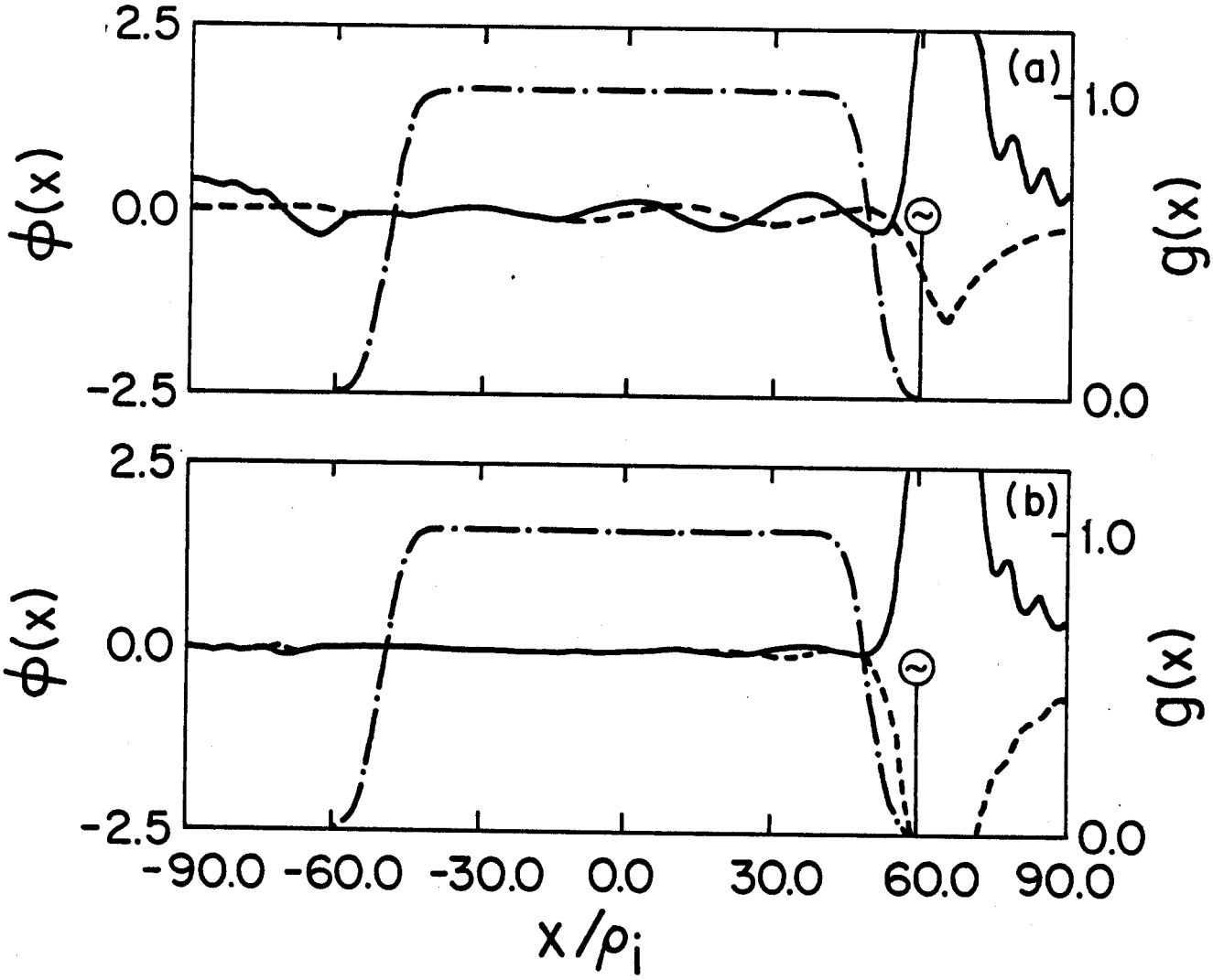
2.5
0.0
-2.5
φ(x)
(a)
1.0
0.0
g(x)
(b)
-90.0 -60.0 -30.0 0.0 30.0 60.0 90.0
x/ρi

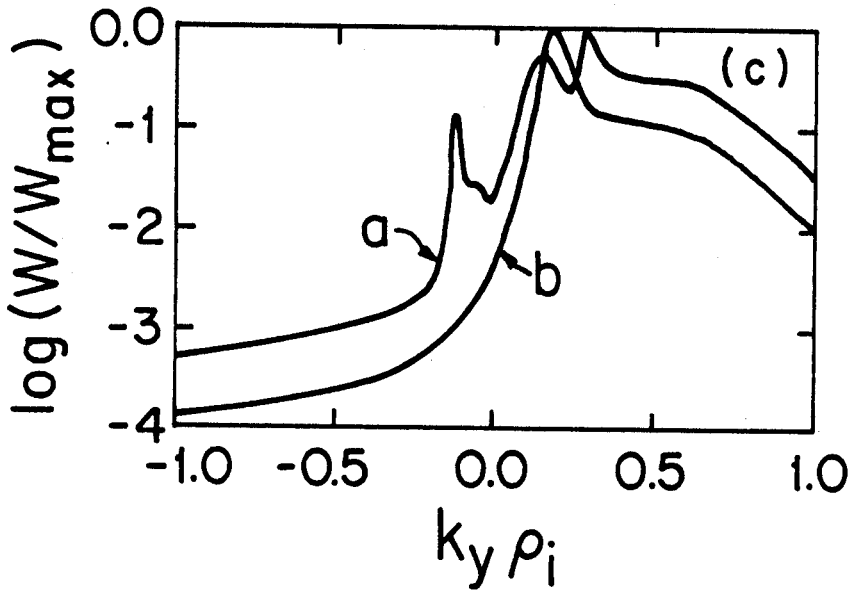
0.0
-1
-2
-3
-4
log(W/Wmax)
(c)
a
b
-1.0 -0.5 0.0 0.5 1.0
ky ρi

Figure 6

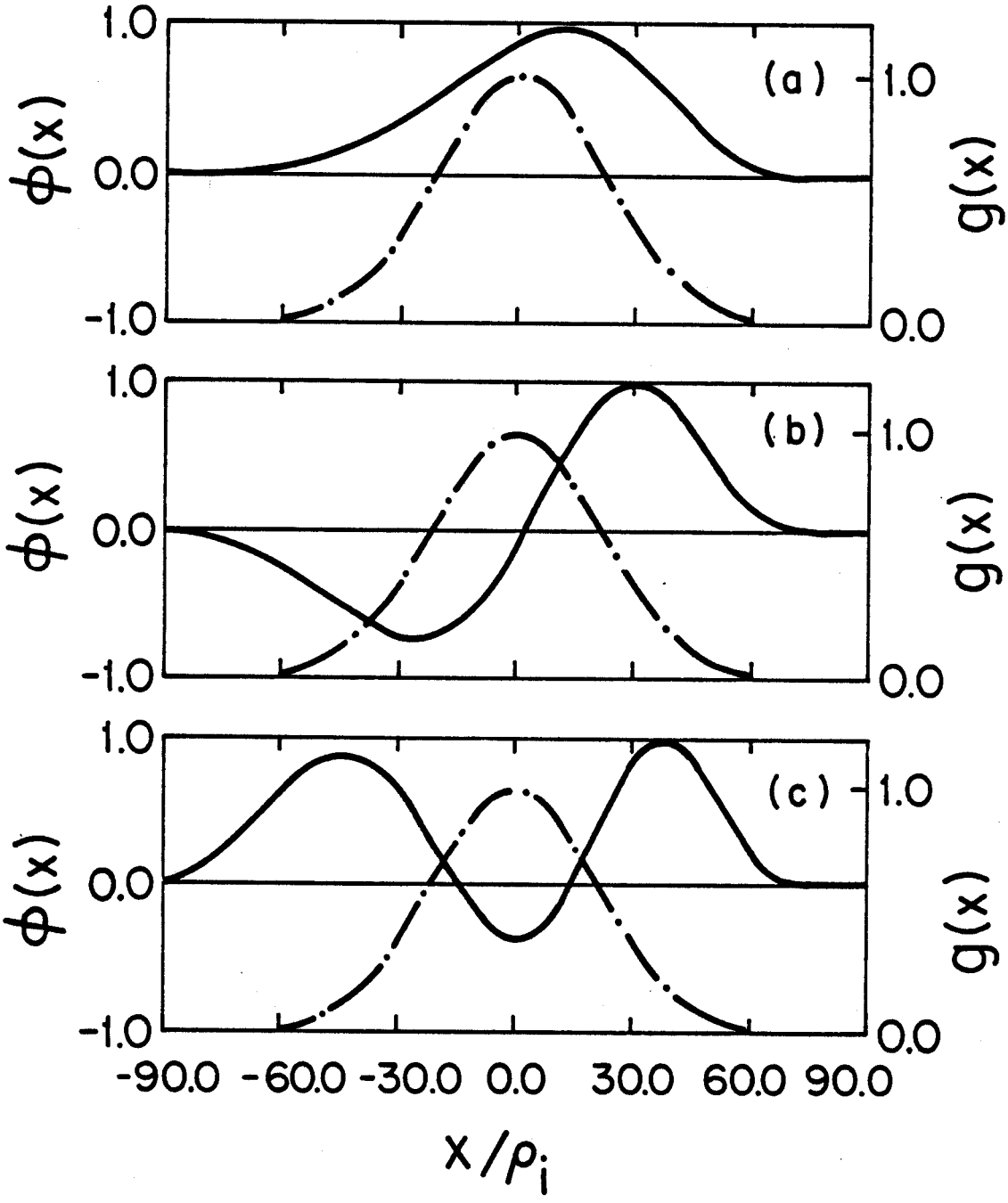

Figure 7

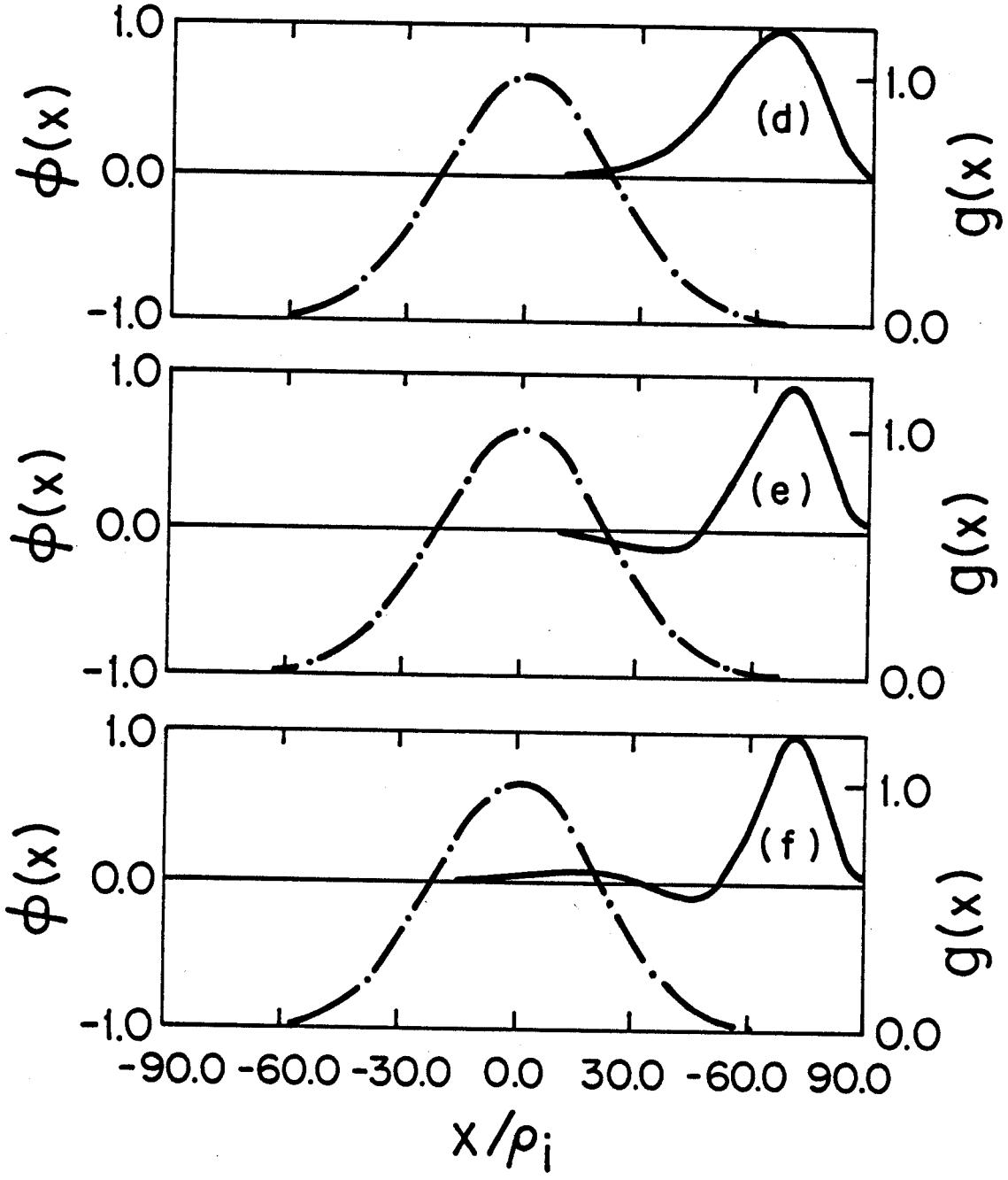

Figure 7

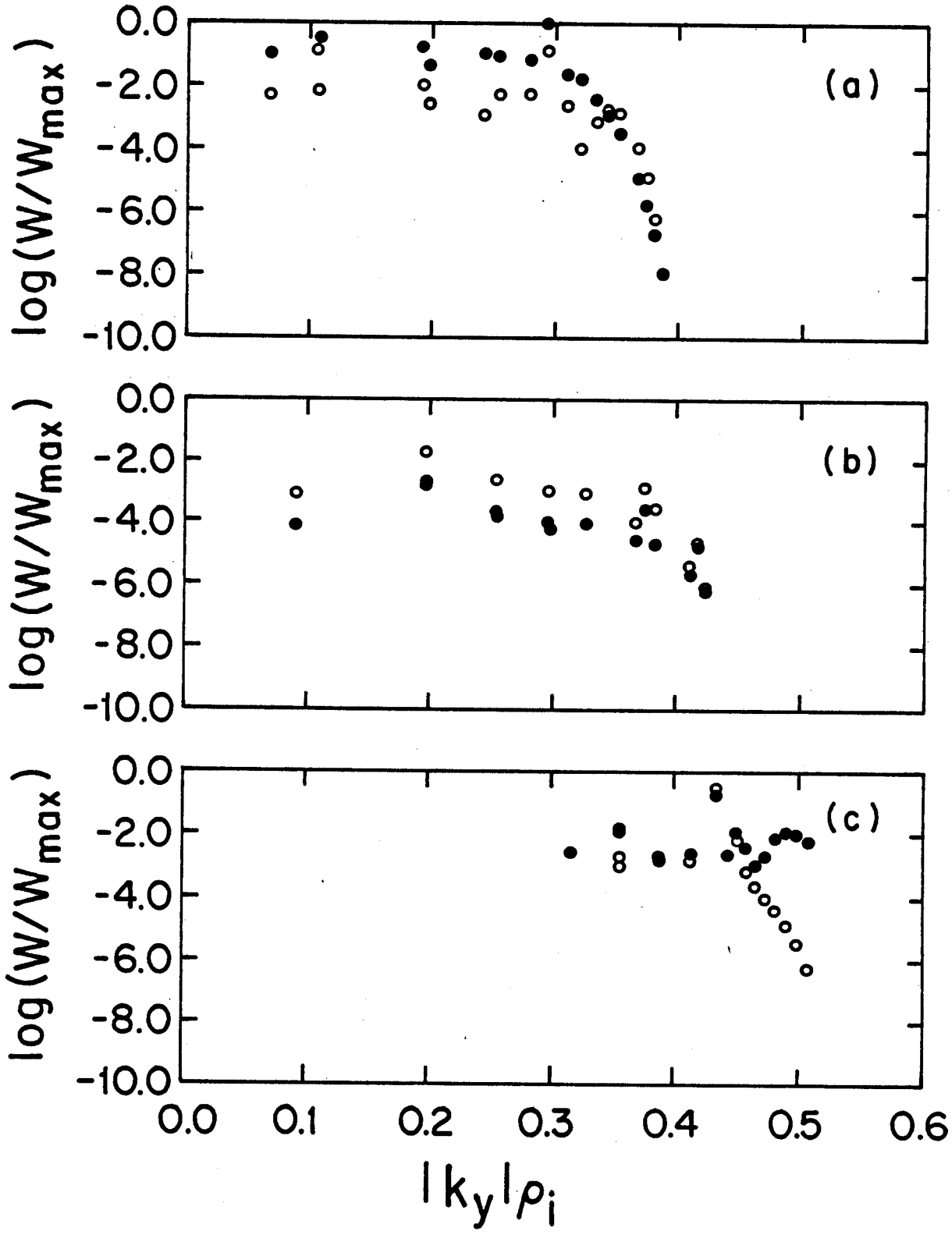

Figure 8

REFERENCES

[1] J.C. Hosea, D. Boyd, N. Bretz, R. Chrien, S. Cohen, P. Colestock, S. Davis, D. Dimock, P. Efthmion, H. Eubank, R. Goldston, L. Grisham, E. Hinnov, H. Hsuan, D. Hwang, F. Jobes, D. Johnson, R. Kaitam J. Lawson, E. Mazzucato, D. McNeill, S. Medley, E. Meservey, D. Mueller, G. Schilling, J. Schivell, G. Schmidt, A. Sivo, F. Stauffer, W. Stoclick, J. Strachan, S. Suckewer, G. Tait, H. Thompson, and G. Zankl, presented at the 8th International Conference on Plasma Physics and Controlled Nuclear Fusion Research, Brussels, Belgium IAEA-CN-38/D-5-1 (1980).

[2] TFR Group, Nucl. Fusion 22, 956 (1982).

[3] N. Hershkowitz, B.A. Nelson, J. Johnson, J.R. Ferron, H. Persing, C. Chan, S.N. Golovato, and J.D. Callen, Phys. Rev. Lett. 55, 947 (1985).

[4] J.R. Ferron, N. Hershkowitz, R.A. Breun, S.N. Golovato, and R. Goulding, Phys. Rev. Lett. 51, 1955 (1983).

[5] T.H. Stix, *The Theory of Plasma Waves*, (McGraw-Hill, New York, 1962).

[6] W.P. Allis, S.J. Buchsbaum, and A. Bers, *Waves in Anisotropic Plasma*, (MIT Press, Cambridge, Massachusetts, 1963).

[7] D.G. Swanson, Phys. Fluids 10, 428 (1967).

[8] J.C. Hosea and R.M. Sinclair, Phys. Fluids 13 , 701 (1970).

[9] B.D. McVey, MIT Report PFC/RR-84-12 (1984).

[10] L. Villard, K. Appert, R. Gruber, and J. Vaclavik, presented at the Third European Workshop on Problems in the Numerical Modeling of Plasmas, LRP 275/85, Varenna, Italy, (1985).

[11] E.F. Jaeger, D.B. Batchelor, and H. Weitzner, ORNL/TM-10204, (1987).

[12] A. Fukuyama, S. Nishikawa, K. Itoh, and S.I. Itoh, Nucl. Fusion 23, 1005 (1982).

[13] B.D. McVey, MIT Report PFC/JA-82-7 (1982).

[14] P.L. Colestock and R.J. Kashuba, Nucl. Fusion 23, 763 (1983).

[15] M. Brambilla, Report IPP-5/15, Garching (1987).

[16] R.L.Guernsey, Phys. Fluids 12, 1852 (1969).

[17] W.L. Waldron , J.L. Shohet, and J.H. Hopps, Phys. Fluids 23, 129 (1980).

[18] R.D. Jones, Phys. Fluids 29, 97 (1986).

[19] A. Sivasubramanian and T. Tang, Phys. Rev. A 6, 2257 (1972).

[20] M. Watanabe, Y. Serizawa, H. Sanuki, and T. Watanabe, J. Phys. Soc. Jpn. 50 1738 (1981).

[21] R. D. Ferraro, R. G. Littlejohn, H. Sanuki, and B. D. Fried, Phys. Fluids 28 2181 (1985).

[22] R. D. Ferraro, R. G. Littlejohn, H. Sanuki, and B. D. Fried, Phys. Fluids 30 1115 (1987).

[23] F. Skiff, M. Ono, P. Colestock, K.L. Wong, Phys. Fluids 28, 2453 (1985).

[24] R. C. Myer, Bulletin of the American Physical Society 27, 8, Part II, 966 (1982).

[25] L. Onsager, Phys. Rev. 37, 405 (1931).

[26] H.B.G. Casimir, Rev. Mod. Phys. 17, 343 (1945).

[27] I. Prigogine, *Introduction to Thermodynamics of Irreversible Processes*, (Interscience Publishers, New York, 1955).

[28] S. Ichimaru, *Basic Principles of Plasma Physics*, (Benjamin/Cummings, Reading, Massachusetts, 1973).

[29] S.G. Mikhlin, *Integral Equations*, (Macmillan, New York, 1964).

[30] M.I. Azbeĺ and E.A. Kaner, Soviet Physics JETP, 5, 730 (1957).

[31] R.D. Ferraro and B.D. Fried, Phys. Fluids 31 2594 (1988).

[32] B.D. Fried and S.D. Conte, *The Plasma Dispersion Function,* (Academic Press Inc., New York, 1961).